

**ELECTRICAL RESISTANCE IN CARBON NANOTUBE – INSULATOR –  
METAL DIODE ARRAYS FOR OPTICAL RECTENNA**

A Thesis  
Presented to  
The Academic Faculty

By

Etizaz Hassan Shah

In Partial Fulfillment  
Of the Requirements for the Degree  
Master of Science in Mechanical Engineering

Georgia Institute of Technology

August 2016

Copyright © Etizaz Hassan Shah 2016

**ELECTRICAL RESISTANCE IN CARBON NANOTUBE – INSULATOR –  
METAL DIODE ARRAYS FOR OPTICAL RECTENNA**

Approved by:

Dr. Baratunde A. Cola, Advisor  
Woodruff School of Mechanical Engineering  
*Georgia Institute of Technology*

Dr. Peter J. Hesketh  
Woodruff School of Mechanical Engineering  
*Georgia Institute of Technology*

Dr. Michael A. Filler  
School of Chemical & Biomolecular Engineering  
*Georgia Institute of Technology*

Date Approved: July 22, 2016

## **Dedication**

All this work is dedicated to my family especially my mother

**Mrs. Najma Naqvi**

and my brother

**Mr. Fakhar Hassan Shah**

for their selfless support throughout my educational career.

## **ACKNOWLEDGEMENTS**

I would humbly thank Dr. Baratunde A. Cola for giving me the lead on this project and having confidence in me while being there for me all the time. After that I would like to specially thank Dr. Virendra Singh for his enormous support throughout this research and Thomas Bougher for his guidance during the experiments. After that, I thank Michael Gaj for the help with metal deposition and Prof. B. Kippelen for providing access to the specialized evaporator. I would also like to thank Dr. Billyde Brown for his help during IV characterization and the rest of the people at NEST Lab for their helpful discussions and comments.

This work was supported by the Army Research Office under Young Investigator Program agreement no. W911NF-13-1- 0491.

# TABLE OF CONTENTS

ACKNOWLEDGEMENTS.....	iv
LIST OF TABLES.....	viii
LIST OF FIGURES.....	ix
SUMMARY.....	xii
CHAPTER 1: INTRODUCTION.....	1
1.1    Motivation.....	1
1.2    Research Objectives and Approach.....	4
CHAPTER 2: RECTENNA BASICS.....	7
2.1    Evolution of Rectenna.....	9
2.2    Variety of Rectenna Designs.....	12
2.2.1    MIM Diodes.....	12
2.2.2    Metal Multi-Insulator Diodes.....	13
2.2.3    Sharp-Tip Diodes.....	15
2.2.4    MIM Travelling-Wave Diode.....	15
2.2.5    Geometric Diodes.....	16
2.3    Multiwall Carbon Nanotube-Oxide-Metal Diode.....	17
CHAPTER 3: EXPERIMENTAL PHASES.....	20
3.1    Phase 1.....	20
3.1.1    Appropriate Thickness for Top Metal.....	20
3.1.2    Opening CNT Tips.....	21
3.2    Phase 2.....	23

3.2.1	Appropriate Thickness for Insulator Layer.....	23
CHAPTER 4:	DEVICE FABRICATION.....	24
4.1	MWCNTs Growth.....	24
4.2	Opening CNTs.....	26
4.3	Oxide Deposition.....	29
4.4	Top Metal Deposition.....	31
CHAPTER 5:	DEVICE CHARACTERIZATION.....	33
5.1	Scanning Electron Microscopy.....	33
5.2	Raman Spectroscopy.....	34
5.3	I-V Characterization.....	36
CHAPTER 6:	RESULTS AND DISCUSSION.....	38
6.1	Phase 1.....	38
6.1.1	Influence of Top Metal Thickness on Contact Resistance.....	38
6.1.2	Sheet Resistance vs. Contact Resistance of Top Metal.....	40
6.1.3	Influence of opening CNT Tips on Contact Resistance.....	41
6.2	Phase 2.....	44
6.2.1	Influence of Insulator Thickness.....	44
CHAPTER 7:	RECTIFICATION PARAMETERS OF DIODE.....	49
7.1	Zero-Bias Resistance.....	49
7.2	Responsivity.....	50
7.3	Asymmetry.....	52
7.4	Coupling Efficiency.....	55
CHAPTER 8:	CONCLUSIONS.....	57

CHAPTER 9: RECOMMENDATIONS.....	59
APPENDIX A: RESISTANCE TABLES.....	61
APPENDIX B: POLYNOMIAL EQUATIONS.....	63
REFERENCES.....	65

## LIST OF TABLES

Table 7.1	Comparison of diode parameters (Conduction is given as an inverse of zero-bias resistance for an ease of description).....	54
Table A.1	Average contact resistances for various top metals and thicknesses.....	61
Table A.2	Percentage change in average contact resistance after opening CNT tips for all four top metals (Ti, Al, Ni, Au) each of 200 nm thickness.....	61
Table A.3	Effect of oxide thicknesses on zero-bias resistance of diodes of Ca/Al, Al, and Au based diodes.....	62

## LIST OF FIGURES

Figure 1.1	Device structure. (a) Schematic of MWCNT-insulator-Metal (insulator is Al <sub>2</sub> O <sub>3</sub> ) optical rectenna and setup for electrical characterization. (b) Enlarged cartoon of single MWCNT-insulator-Metal diode and the associated electrical resistance network.....5
Figure 2.1	Block diagram of rectenna.....7
Figure 2.2	Block diagram of optical rectenna.....8
Figure 2.3	Demonstration of the rectenna helicopter on Oct 1964.....10
Figure 2.4	Energy band diagram for the resonant and step multi-insulator diodes: Forward and reverse bias profiles are shown respectively in (a) and (c) for the resonant, and in (b) and (d) for the step diode. The dotted thinner lines show the profiles with barrier lowering [1].....14
Figure 2.5	(a) Isometric view of rectenna with traveling-wave MIM diode (b) 3D view of the traveling-wave MIM diode with surface-plasmon depleting along the waveguide.....16
Figure 2.6	(a) Schematic diagram of a geometric diode theory of operation. (b) SEM image of a graphene geometric diode.....16
Figure 2.7	Schematic of the vertically aligned MWCNT- Al <sub>2</sub> O <sub>3</sub> -Ca optical rectenna by Cola.....18
Figure 3.1	SEM image of vertically aligned MWCNT film (left) and high magnification cross-section images of 200 nm Au/MWCNT interface, where tubes are dangling above forest (middle), and plasma treated forest (right).....21
Figure 3.2	SEM images of MWCNTs (left) before and (middle) after O <sub>2</sub> plasma etch at 80W for 30s, and (right) 60s at (a) high magnification (b) lower magnification, and (c) lowest magnification with cross-section view.....22
Figure 4.1	Multiwall carbon nanotube growth processes by chemical vapor deposition, (a) tip growth (b) root growth.....25
Figure 4.2	SEM of sample 1.....27
Figure 4.3	SEM of sample 2.....28
Figure 4.4	Step by step demonstration of oxide deposition using Atomic Layer Deposition (ALD).....30

Figure 4.5	Top metal blankets over the MWCNTs.....	31
Figure 4.6	Block diagram of complete fabrication process of MWCNT-Al <sub>2</sub> O <sub>3</sub> -Metal rectenna over 1X1 inch substrate.....	32
Figure 5.1	Top down SEM images of (a) 200 nm Ti, (b) 200 nm Ni, (c) 200 nm Al and (d) 200 nm Au coated closed tip MWCNTs.....	34
Figure 5.2	Effects of oxygen plasma etch on Raman I <sub>G</sub> /I <sub>D</sub> ratio: as-deposited MWCNTs (red curve), after 80 W plasma etch for 30 seconds (black curve) and 90 seconds (blue curve).....	35
Figure 5.3	Schematics of 4-probe resistivity measurement system (red arrows show the flow of current).....	37
Figure 6.1	Influence of the choice of top metals (Ti, Al, Ni and Au) and their thickness on I-V characteristics: I-V plots for (a) 50 nm, (b) 200 nm, and (c) 500 nm top metal thickness samples.....	39
Figure 6.2	Plot of average contact resistance for various top metal thicknesses.....	40
Figure 6.3	Four-point probe IV curves showing sheet resistance of top metals (200 nm Ti, Al, Ni and Au).....	41
Figure 6.4	I-V plots of (a) closed and (b) open tip MWCNTs with 200 nm top metal thicknesses. Inset shows I-V curve with expanded voltage range for Al top metal that exhibits significant non-linearity.....	42
Figure 6.5	Percentage change in average contact resistance after opening CNT tips for all four top metals (Ti, Al, Ni, Au) each of 200 nm thickness.....	43
Figure 6.6	Influence of oxide thickness and top metal workfunction on I-V characteristics of MWCNT-I-M diodes: Diodes have (a) 50nm Ca / 60 nm Al / 90 nm Ag, (b) 60 nm Al / 90 nm Ag, and (c) 200 nm Au top metal layers. (90 nm Ag layer is just the filling layer to reach the optimized thickness).....	45
Figure 6.7	Diode resistance vs. voltage for devices with: (a) 50 nm Ca / 60 nm Al / 90 nm Ag, (b) 60 nm Al / 90 nm Ag, and (c) 200 nm Au top metal layers. (Insets are zoomed in).....	46
Figure 7.1	Effect of oxide thickness on zero-bias resistance of diodes.....	49
Figure. 7.2	Responsivity plots for devices with (a) 50 nm Ca / 60 nm Al / 90 nm Ag, (b) 60 nm Al / 90 nm Ag, and (c) 200 nm Au top metal layers, respectively.....	51

Figure. 7.3 Asymmetry plots for devices with (a) 50 nm Ca / 60 nm Al / 90 nm Ag,  
(b) 60 nm Al / 90 nm Ag, and (c) 200 nm Au top metal layers,  
respectively.....53

## SUMMARY

Vertical tunnel diode arrays made from multiwall carbon nanotubes (MWCNTs) have shown recent promise for developing a practical optical rectenna, which is a device to convert electromagnetic waves at optical frequencies to direct current. Realizing an optical rectenna requires an antenna to be coupled to a diode that operates on the order of PHz (switching speed on the order of fs). Previously, we have demonstrated an optical rectenna device by engineering MWCNT-insulator-metal (MWCNT-I-M) tunnel diodes at the tips of vertically aligned MWCNT arrays, which act collectively as the antenna. However, the high electrical resistance of the MWCNT-I-M diode resulted in poor impedance matching between diode and antenna, which limited the rectified power. Here, we address this issue of impedance mismatch through a series of experiments designed to elucidate contributions to the total electrical resistance of the device. Different combinations of metals, and metal and insulator thicknesses were tested for reduced contact resistance, while maintaining a working diode. Another development towards reducing resistance was to open MWCNT tips using oxygen plasma, which exposed multiple walls for bonding rather than just outer wall of closed tip CNTs. These developments were combined to reduce zero-bias resistance of MWCNT-I-M diode arrays to as low as  $100 \Omega\text{cm}^2$ , which is 75 times lower than in our previous report.

# CHAPTER 1

## INTRODUCTION

### 1.1 Motivation

Harvesting renewable resources to their full extent has been the key topic in the 20<sup>th</sup> century amid to the environmental concerns and depletion of fossil fuels. Out of all the green resources, solar energy has been focused and developed the most, as the sun is constant source of energy. Photovoltaic (PV) solar cells have been the conventional solar energy harvesters with a huge success after the development of silicon solar cells at Bell Laboratories in 1954 [2]. But these PV cells as discussed by Shockley and Queisser are limited to 30% efficiency for single-junction [3] and 55% for multi-junction solar cell under specific conditions [4]. The concept of rectenna (RECTifying antENNA) as an “Electromagnetic Wave Energy Converter” evolved in the wake of these efficiency limitations faced by semi-conductor solar cells. Bailey devised the idea of this wave absorber-convertor and expected it to be a catalyst in this arena of science [5]. Recent intensive research on rectenna is the fulfillment of his expectation. Rectenna has been researched as the technology with efficiencies exceeding the Shockley–Queisser limits. Starting from the microwave regime [6], rectenna devices have now entered into the regime of faster optical frequencies [7] while many new antenna and diode technologies have been developed along the way [8-16].

Rectenna solar cell technology has many factors making it favorable over conventional solar cells [17]. The following are the major ones:

- Ultimate efficiency of rectenna solar cells is as high as that of conventional PV cells and possibly higher even without a ‘photon homogenizer’ i.e., without down - converting or mixing. It has been observed on the base theory of PAT (Photon assisted Tunneling) that, for diodes that are optimally matched to antennas, monochromatic power conversion efficiencies approach 100% and the multispectral efficiency is limited to 44% at solar terrestrial intensities [18]. However mixing occurs in microwave rectennas and down - converting occurs in thermo-photovoltaic (TPV) rectenna cells. Mixing helps raise overall efficiency even more.
- Incorporating different wavelength is a lot cheaper and easier in rectenna than in multi-junction solar cells. In conventional PV cells, this requires semiconductors of different band gaps, which make it expensive and incompatible most of the time. But in the case of rectenna, it can be done easily by tweaking the size of the antenna and shifting the operating voltage to change the wavelength of peak sensitivity.
- The material for the rectenna is available and is cheaper in the thin film form. Processing of the material can be cheaply controlled with innovative technologies available.
- An interesting application of rectenna is its use for waste heat harvesting. It is easier for the rectenna to harvest the lower frequency heat waves than higher frequency visible light as it relaxes the RC time constant condition. Whereas, conventional PV cells cannot incorporate longer wavelengths of heat and the

thermoelectric devices are expensive and inefficient as compared to rectenna solar cells.

- Using the heat harvesting capability of the rectenna solar cells, they can be a help to the thermo-photovoltaic systems. In TPV, the sun heats up an absorber, which radiates the lower temperature blackbody spectrum onto the narrow band-gap solar cells. Rather than using expensive narrow band-gap semiconductor solar cells, rectenna cells can be used which work even more efficiently at low frequency infrareds emitted by the absorber.

With all these perks of rectenna solar cells, there are still developmental issues causing a hurdle in the commercialization of this amazing technology. The following are some notable issues:

- Impedance of the diode must match the impedance of antenna for efficient power transfer [19]. Antenna resistance is normally on the order of a few hundred ohms at visible light, while diodes of enough responsivity haven't reached to this lower resistance.
- RC time-constant is the decisive parameter for the rectenna to operate on visible light. For visible light rectification, the RC time constant should be less than  $\sim 0.1$  fs. While for the diode which matches the antenna resistance, it is very difficult to provide a sufficiently small capacitance. Planar diodes can't reach there thus diodes which can cope with the RC limitation of the parallel plate diodes are required and some designs of such diodes are under research.
- The antenna part of the rectenna has reached to a stable stage with good solutions available but some issues still persist. E.g. efficiently absorbing all the incident

radiations while maintaining constant impedance to match with the diode, keeping resistance losses low at terahertz frequencies where metals become more resistive are some of the issues to be addressed.

Considering the extensive research already being done on antennas and plasmonic enhancement being the potential solution for much of the above mentioned antenna issues, we focused on the diode side of the rectenna. Previously we have demonstrated an optical rectenna device by engineering multiwall carbon nanotube – insulator - metal (MWCNT-I-M) tunnel diode at the tip of a vertically aligned MWCNT, which acts as the antenna [7]. But the high electrical resistance of the MWCNT-I-M diode caused poor impedance matching between diode and antenna, which resulted in limiting the rectified power. Here, we address this issue of impedance mismatch through a series of experiments designed to elucidate contributions to the total electrical resistance of the device.

## **1.2 Research Objectives and Approach**

Our design of multiwall carbon nanotube (MWCNT)-based optical rectenna in which the antenna itself is an integral part of the diode is a natural approach for efficient antenna-diode coupling [5], [8], [19]. In our device, the diode is engineered on the tip of a 10  $\mu\text{m}$  vertically aligned CNT; see Figure 1.1(a). The CNT works as an antenna [20], [21] and also plays the role of one of the metals in MWCNT-insulator-metal (MWCNT-I-M) diode. MWCNTs are grown using low-pressure chemical vapor deposition (LPCVD) and are subsequently coated with a thin layer of  $\text{Al}_2\text{O}_3$  using atomic layer deposition (ALD). This  $\text{Al}_2\text{O}_3$  layer serves as an insulator in the diode. Finally, a low-workfunction top

metal is thermally evaporated on the top of Al<sub>2</sub>O<sub>3</sub>-coated CNT tip to complete the rectenna device. The enlarged cartoon in Figure 1.1(a) shows the basic structure of single CNT optical rectenna.

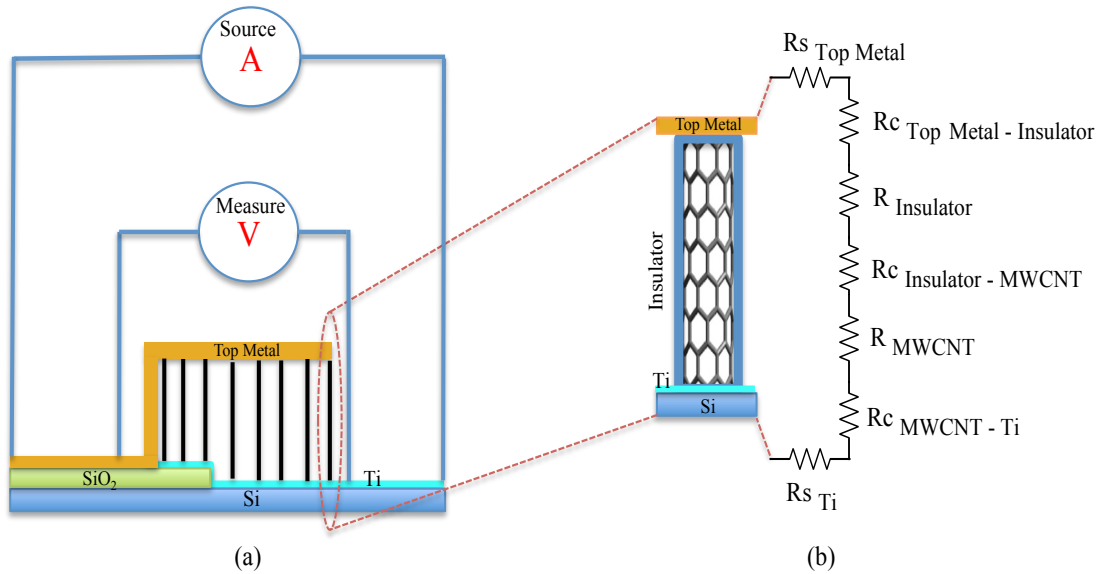


**Figure 1.1** Device structure. (a) Schematic of MWCNT-insulator-Metal (insulator is Al<sub>2</sub>O<sub>3</sub>) optical rectenna and setup for electrical characterization. (b) Enlarged cartoon of single MWCNT-insulator-Metal diode and the associated electrical resistance network.

This study has been designed to identify and address the factors contributing towards high electrical resistance in MWCNT-I-M diode. Figure 1.1(b) is a schematic of all the electrical resistances involved in the diode. Analyzing all these resistances individually has helped us in understanding the major contributors in diode resistance. Resistance at the CNT and insulator interface i.e. R<sub>c</sub> Insulator-MWCNT is one of the vital contributors towards overall diode resistance as it influences the rectification performance of the diode. CNT morphology and quality of the insulator coating on CNT are the decisive factors for this interface. Typically, the tips of as-deposited MWCNTs have a

hemispherical graphite cap. This cap makes only the outer layer of MWCNT exposed to bonding while limiting the inner walls' bonding sites. Thus removing the cap will expose multiple conductivity walls, which leads to a low-resistance ohmic contact [22]. The second contributor towards diode resistance is insulator thickness [23]. Insulator thickness affects the barrier height and consequently the turn on voltage and tunneling current. It also plays an important role in diode capacitance,  $C_D$  as  $C_D = \epsilon_0 \epsilon A/d$  [24], where  $\epsilon_0$  is the permittivity of the vacuum,  $\epsilon$  is the relative permittivity of the insulator,  $A$  is the cross-sectional area of the diode and  $d$  is the insulator thickness. Diode capacitance is the main factor in computing cutoff frequency i.e.  $f_c = 1/(2\pi RC)$ . So determining the insulator thickness is a key factor for a fast tunneling diode. Thirdly, the insulator and top metal interface also plays its role in diode resistance. To address this, thickness and composition of top-metal is optimized carefully considering its impact on diode resistance and rectification/asymmetry.

## CHAPTER 2

### RECTENNA BASICS

An important thing to understand is the difference between solar cells and rectenna. Basically, both absorb photons to generate direct current (DC). But their principle of operation is substantially different. Solar cells are based on Einstein's view of the photon and are designed based on quantum physics [25], where light is perceived in its particle form. Solar cells cannot absorb low energy photons and higher than band-gap energy photons are wasted in the form of heat loss. While rectenna is based on Maxwell's electromagnetic waves [17]. Rectenna efficiency is limited by the cutoff frequency i.e. any wave below this frequency can be harvested.

Basic components of the rectenna device are shown in the Figure 2.1. These components are associated with a rectenna operating at microwave frequencies.

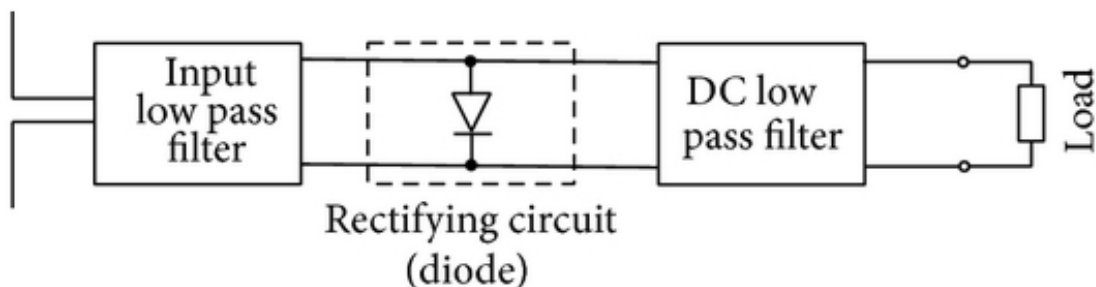


**Figure 2.1:** Block diagram of rectenna

The antenna captures the incoming microwaves and the electric field from these incident electromagnetic waves induces an alternating current (AC) in the conducting antenna. A

low-pass filter is used for the impedance match between the antenna and the rectifier. The filter also suppresses the high order harmonics produced by rectifier (diode) [26]. The diode rectifies the input AC signal the DC used by the load. The DC pass filter smoothens the rectified signal from diode for efficient transfer to the load [27].

Rectenna size varies according to the frequencies it operates on. Mainly the antenna dimensions are of the same scale as the operational frequency [28]. Thus for microwave frequencies, the antenna is a bit bigger compared to the infrared or optical range. For optical rectenna, due to its smaller size, it is difficult to incorporate the filters thus optical/solar rectenna consists of only antenna and diode as show in Figure 2.2 [29].

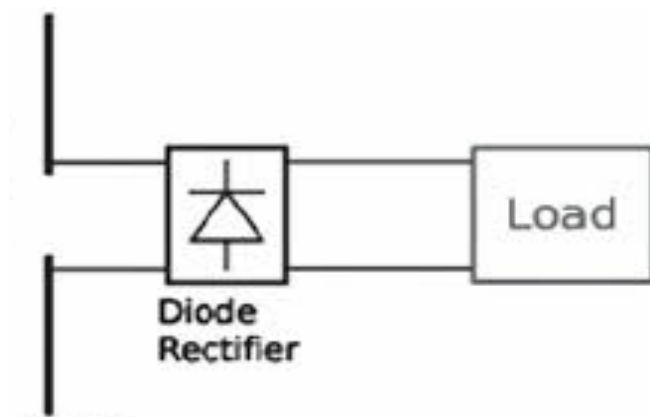


**Figure 2.2:** Block diagram of optical rectenna

Removing low pass filter helps harvesting the frequencies up to cutoff frequency but at the same time it causes the impedance mismatch between antenna and diode, which results in cutting the efficiency down [19].

## 2.1 Evolution of Rectenna

William Brown is considered the pioneer of the rectenna. He used rectenna for wireless power transmission in 1960s [6]. The major issue that he was facing for microwave power transmission (MPT) was to find an efficient way of converting incoming microwaves to DC power. However, wireless power transmission wasn't a new concept as Tesla has demonstrated it in 1899 [30]. Raytheon Company, where Brown was working, proposed Raytheon Airborne Microwave Platform concept to the US Department of Defense in 1959 for the communication and surveillance applications [31] but the Department of Defense denied the funding. However, the company continued the research on this project. One missing thing was a suitable microwave rectifier, which could convert the microwaves to DC for the motors on platform. 'They used horn-illuminated ellipsoidal reflector that focused the microwave beam into the horn at a 20 feet distance, where they were converted to DC power by the rectifier' [19]. In 1963, Brown discussed the issue with Roscoe George, who had experience with microwave point-contact semiconductor diodes. Following their experimentation, 'rectenna' was invented and patented later in 1969. Based on this, Brown built a helicopter, which flew 60 feet above a transmitting microwave for 10 hours (Figure 2.3).

After this development, MPT became a popular topic and different applications triggered the research in this new area. One of these is an idea proposed by Glaser for the solar power satellite (SPS) in 1968 [32]. SPS is the idea of a power station on the geostationary orbit, which collects solar power and transmits the microwaves of the 2.54 GHz band to a rectenna array on the ground. Brown and Glaser worked together on this project for three

years and it was called “DOE/NASA Satellite Power System Concept Development and Evaluation Program” [33].



**Figure 2.3:** Demonstration of the rectenna helicopter on Oct 1964

The work ended in 1980 with a lot of developments in rectenna and transmission technology but it couldn't secure more funding. However, some studies were carried out in Yamasaki, Japan later in 1990s [34, 35].

However the SPS project led towards other applications, such as inter-satellite power transmission for mechanical actuators and short distance power transmission between different parts of satellites [36-39], RFID and biomedical implants [40]. For data communication systems, printed rectenna for DC power supply has also been reported in literature [41].

R.L Bailey explored a new area of application for rectenna i.e. exploiting the wave nature of light, which was a summer project of NASA in 1960s [42]. He suggested a conical structure for antennas to replicate the natural antennas in insects, which was similar to dielectric rod antennas. He called his device ‘electromagnetic wave energy converter (EWEC)’ and published it in 1970 [5]. Fundamentally, this device was similar to what Brown suggested but Bailey designed it a way that it works on higher frequencies and he referred to it as a solar rectenna. Bailey and Fletcher worked together, they indicated the importance of optimization of antenna design and major challenges regarding the rectification in their final report published in 1975 [43].

After Bailey, Marks contributed a lot to the rectenna research with his proposed structures [13, 44-46] inspired by the half-wave rectifier EWEC. Marks was the one who invented antenna-like cylinders attached to metal-insulator-metal diodes.

In 1974, Gustafson and Billman were the first who suggested using visible light and they formed the base for optical diodes [47]. In 1996, Lin et al. were the first to give an experimental evidence of rectenna operating in visible light range frequency [14]. Their parallel dipole sub-nanostructures connected to a p-n junction for rectification recorded a short circuit current.

Currently, Patrick Pinhero from University of Missouri [48]; Matteo Pasquali from Rice University [49], Brian Willis from University of Connecticut [50], Garret Moddel from University of Colorado and Baratunde Cola of Georgia Institute of Technology are the key players in the optical rectenna (also called Nantenna). A breakthrough is reported by Baratunde Cola of Georgia Institute of Technology, as he was successfully able to demonstrate an optical rectenna practically [7]. Cola et al. introduced multiwall carbon

nanotubes (MWCNTs) as antenna and substituted nanotubes as one of the metals of MIM diode. Their MWCNT-insulator-Ca is claimed to be the world's fastest MIM tunneling diode, capable of rectifying terahertz frequencies. Individual junctions have a capacitance of only 1.7 atto-farads, with switching time on the order of 1 femtosecond. The work in this thesis is the extension of work done by Cola so far.

## **2.2 Variety of Rectenna Designs**

Nowadays, a lot of research is being done on rectenna devices and different results originate from different groups based on the design of their device. The focus is to find an appropriate rectenna design which can harvest visible light which requires  $\sim 0.1$  fs RC time constant that requires very small resistance and capacitance of diode which also leads towards impedance match between the antenna and diode as it is necessary for an efficient power transfer. In contrast to the optical diodes, there are fewer impediments in the development of efficient optical antennas as antennas have already been researched a lot and are mostly functioning at visible frequencies. Thus, it is important to discuss different approaches being pursued in the diode designs in today's research.

### **2.2.1 MIM Diodes**

An MIM diode is made of two metal electrodes with an extremely thin (few nanometers) insulator layer in-between. In MIM diodes the metals have a higher workfunction than the electron affinity of the insulator producing a barrier at the metal-insulator interface. Electron tunneling occurs in femtoseconds in MIM diodes [51], which helps MIM diodes to operate at the terahertz frequencies in the visible region. In the past, MIM diodes were

used to be made by pressing a thin metal wire against the oxidized sheet of metal [52]. However, recent developments in the lithography techniques have helped making MIM diodes more reliably. Simply oxidizing the metal can grow a thin layer of oxide. Developments in atomic layer deposition made this even easier for metal or oxide deposition in nanometer range [53].

However, the large RC time constant eliminates the possibility of using parallel plate MIM diodes for the rectification of visible light [54, 55]. They can work on low terahertz frequencies but for higher frequencies their response is not efficient. But our design of MIM diode [7] is interestingly different which made them perfect to use for visible light rectification.

### **2.2.2 Metal Multi-Insulator Metal Diodes**

Instead of a single insulator layer between the metals, multiple layers can be incorporated to make a multi-insulator metal diode. Normally two insulator layers of different electron affinity are used to make metal-insulator-insulator-metal (MIIM) diodes. These diodes were introduced by Phiar Corp and patented by Moddel [56, 57]. MIIM diodes have shown a 10 times higher responsivity than a derivative MIM diode as IR detectors [58]. Maraghechi et al. [59] have recorded 10 times improvement in the non-linearity for their Cr/Al<sub>2</sub>O<sub>3</sub>/HfO<sub>2</sub>/Cr diode compared to the Cr/Al<sub>2</sub>O<sub>3</sub>/Cr and Cr/HfO<sub>2</sub>/Cr diode. Non-linearity enhancement in these multi insulator diodes is attributed to two mechanisms. One is the formation of a resonant well between insulating layers as shown in Figure 2.4 (a, c), which increases the tunneling when Fermi level reaches the resonant energy by the applied voltage. And the second reason is the formation of a step in the insulator

conducting band edges as shown in Figure 2.4(b, d), in a way that electrons tunnel through both insulators for one voltage and just one insulator for the other voltage polarity. Moddel et al. [1] have proved this, for their W/Nb<sub>2</sub>O<sub>5</sub>/Ta<sub>2</sub>O<sub>5</sub>/W MIIM diode compared to W/Nb<sub>2</sub>O<sub>5</sub> on one side and a W/Ta<sub>2</sub>O<sub>5</sub> on the other side MIM diodes.

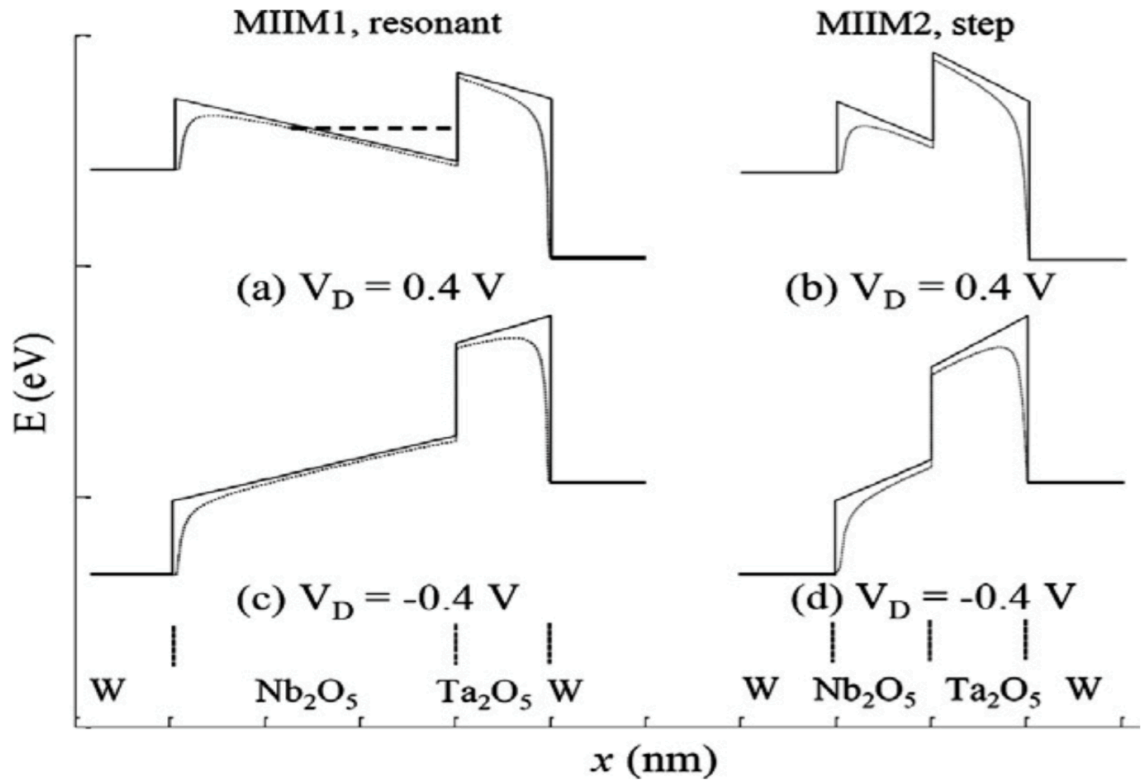


**Figure 2.4.** Energy band diagram for the resonant and step multi-insulator diodes: Forward and reverse bias profiles are shown respectively in (a) and (c) for the resonant, and in (b) and (d) for the step diode. The dotted thinner lines show the profiles with barrier lowering [1].

Although MIIM diodes have shown improvements over the MIM diodes, they still face the issue of fundamental RC limitations.

### **2.2.3 Sharp-Tip Diodes**

To address the RC timing constant issues faced by MIM and MIIM diodes, a new structure of incorporating the vacuum instead of the insulator layer have been suggested and tested. So these sharp-tip diodes become metal-vacuum-metal (MVM) diodes. In parallel plate planer MIM diodes, RC is independent of the area while in MVM, for spherical tips the RC varies with the square root of the area [17]. That's why the response time decreases proportionally to the tip radius. The major issue is controlling this gap/vacuum and keeping it within the nanometer range.

However, Miskovsky et al. [60] is believed to have tackled this issue by using ALD for metal layers deposition.

### **2.2.4 MIM Traveling-Wave Diodes**

In a traveling-wave diode the RC characteristics are controlled mainly by the geometry rather than electron tunneling properties in MIM diodes. In this traveling wave rectenna, the MIM junction is situated between the two arms of bow-tie antenna as shown in the Figure 2.5(a) [61], which allows the diode to rectify the absorbed radiation efficiently at the junction. As diode and antenna are very close, it reduces losses [62]. This design is similar to the bow-tie antenna except that, there is a thin insulator layer in-between, which forms the extended MIM wave-guide; see Figure 2.5(b).

The absorbed radiation travels down the MIM diode in the shape of surface plasmons and the current induced between metals results in tunneling of the electrons. Moddel et al. [63] proposed the MIM traveling-wave structure and tested it for 10 and 1.5  $\mu\text{m}$  wavelengths. IBM used this approach successfully as traveling-wave structure over the

Si-SiO<sub>2</sub> waveguide [12]. However, the resistive losses in the metal waveguide structure can bolt down a lot of plasmon energy.

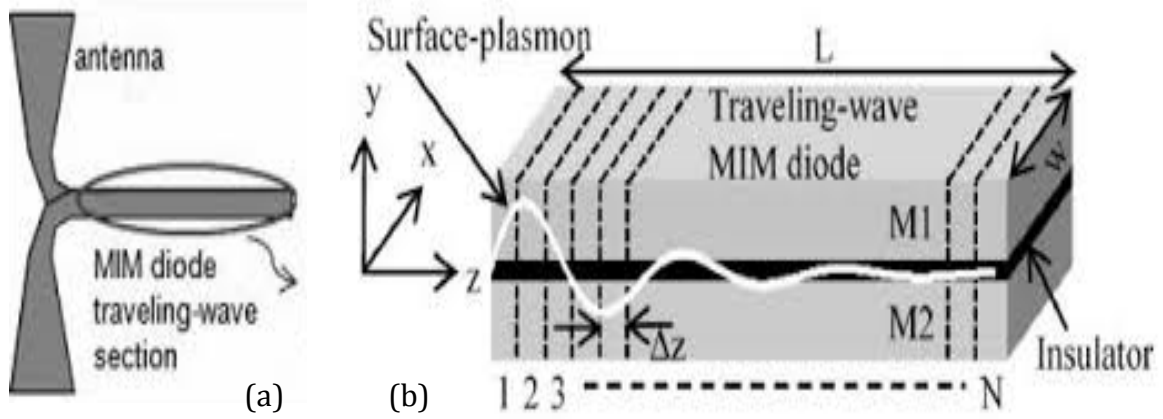


**Figure 2.5.** (a) Isometric view of rectenna with traveling-wave MIM diode (b) 3D view of the traveling-wave MIM diode with surface-plasmon depletion along the waveguide

### 2.2.5 Geometric Diodes

In geometric diodes, it is the geometry of the device that decides the asymmetry rather than the electronic band structure. Model conceived the idea of the geometric diode [64]. The diode consists of the thin film patterned into an inverse arrowhead configuration as shown in the Figure 2.6 [65].

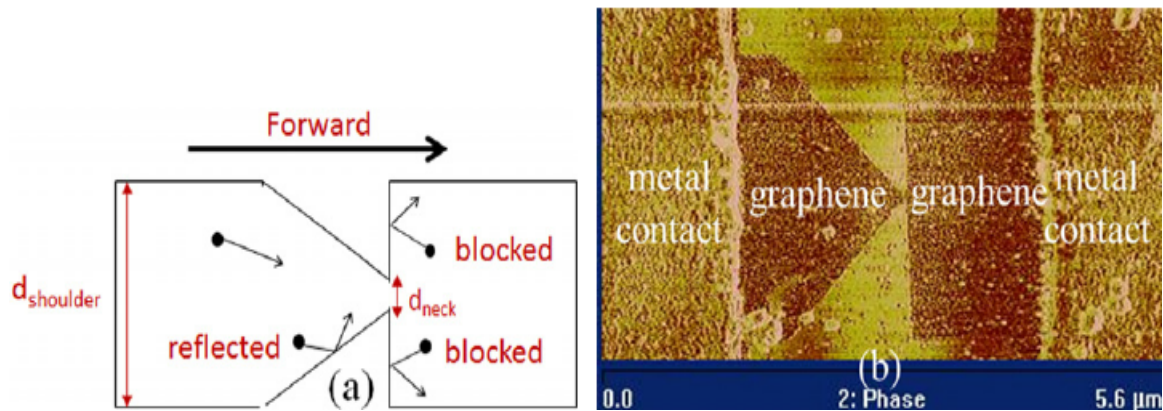


**Figure 2.6.** (a) Schematic diagram of a geometric diode theory of operation. (b) SEM image of a graphene geometric diode

The width of the neck (channel opening) is of crucial importance in this design as it should be of the same magnitude as the mean-free path length (MFPL) of the thin film material for the efficient rectification [66-69]. The probability of electrons passing from the left to the right is much higher than the probability of them passing from the right to the left due to the funneling effect of the sloped edges. Such devices have small capacitance because of being the planar structure. Since they are made of conducting films, their resistance can be easily matched to the antenna resistance of efficient coupling, thus giving lower RC time constant.

However, as described earlier, for the rectification the critical dimension of the neck should be similar to the MFPL. Graphene has been used for this purpose but it has not shown encouraging results for the visible light rectification as of compromised electronic properties of graphene during standard nanofabrication processing.

### **2.3    Multiwall Carbon Nanotube - Oxide - Metal Diode**

The emergence of nanomaterials offers significant promise in alleviating the limitations on rectenna mentioned above. In particular, CNTs have been shown to provide exceptional functional performance in nanoelectronics and sensing applications. Arrays of aligned multiwall CNTs have been shown to demonstrate antenna like interaction with electromagnetic radiation [21]. The multiwall CNTs exhibited both polarization and the length antenna effects that could be used in rectennas for IR and optical detection and solar harvesting applications [70]. A combination of these novel optical and electrical properties together with a tunable range of work function (4.6 eV – 5.05 eV) depending upon diameter, length, arrangement and doping effects in the nanotubes, MWCNTs

showed immense potential for developing vertical MIM diodes for candidate applications [71, 72]. So Cola et al. at their NanoEngineered Systems and Transport (NEST) Lab introduced multiwall carbon nanotubes (MWCNTs) as antenna and substituted nanotubes as one of the metals of MIM diode (Figure 2.7). Their MWCNT- $\text{Al}_2\text{O}_3$ -Ca is claimed to be the world's fastest MIM tunneling diode, capable of rectifying terahertz frequencies. Individual junctions have a capacitance of only 1.7 atto-farads, with switching time on the order of 1 femtosecond [7]. MWCNT based diode perfectly aligns with rectenna principle of directly rectifying electromagnetic waves captured by antenna rather than reported principle of photo-detection based on hot electron decay in a plasmonic nanoscale antenna[73, 74].

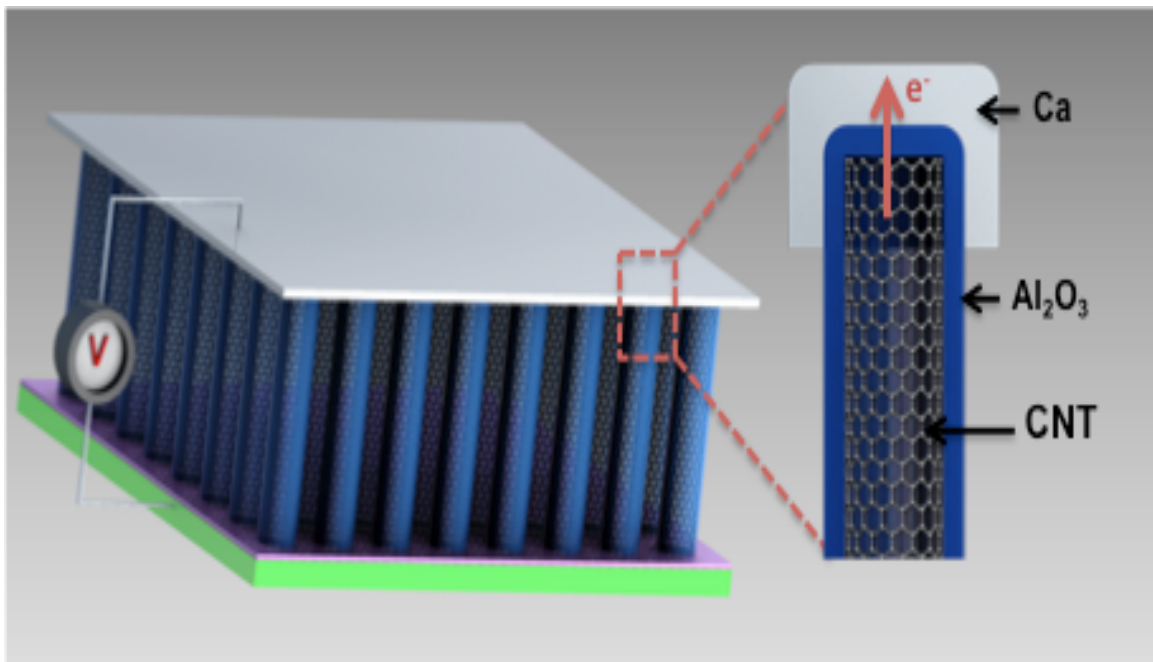


**Figure 2.7.** Schematic of the vertically aligned MWCNT-  $\text{Al}_2\text{O}_3$ -Ca optical rectenna by Cola

The work in this thesis is an extension of the previous work done by Cola. A lot of emphasis has been laid on the reduction in diode resistance to efficiently couple it with the antenna. In this regard, the study has been divided into different phases. All the resistances contributing towards the total resistance of the diode have been studied step-by-step to identify the factors contributing towards the higher resistance.

## **CHAPTER 3**

### **EXPERIMENTAL PHASES**

Different approaches were utilized to find the best combination of metal, CNT and oxide parameters to better understand and optimize contact and sheet resistances. The study was conducted in two phases.

#### **3.1 Phase 1**

The first phase was designed to understand metal contact resistance to our MWCNT arrays, and characterize the role of sheet resistance ( $R_s$ ) of a metal film deposited atop CNT tips. For this phase, the complete structure shown in Figure 1.1(a) was fabricated, but without using  $Al_2O_3$  layer. This phase was designed to find an appropriate thickness of top metal and mainly to understand the effect of opening CNT tips on the metal-CNT contact resistance.

##### **3.1.1 Appropriate Thickness for Top Metal**

Four different top metals Ti, Al, Ni, and Au were deposited over closed tip CNTs to measure contact resistance of each metal with MWCNTs. Each metal was deposited with three different thicknesses of 50, 200 and 500 nm (i.e., 12 devices in total) to understand the impact of thickness on the sheet resistance and to visualize the conformity of metal coating over CNTs.

### 3.1.2 Opening CNT Tips

After examination of the impact of metals and their thicknesses, the effect of opening CNT tips was measured. The caps of MWCNTs were removed using 80 W oxygen plasma and four different etching times: 30, 60, 90 and 120 s. The O<sub>2</sub> plasma helped to improve the CNT forest alignment while etching away tangling tubes above the forest, see Figure 3.1.

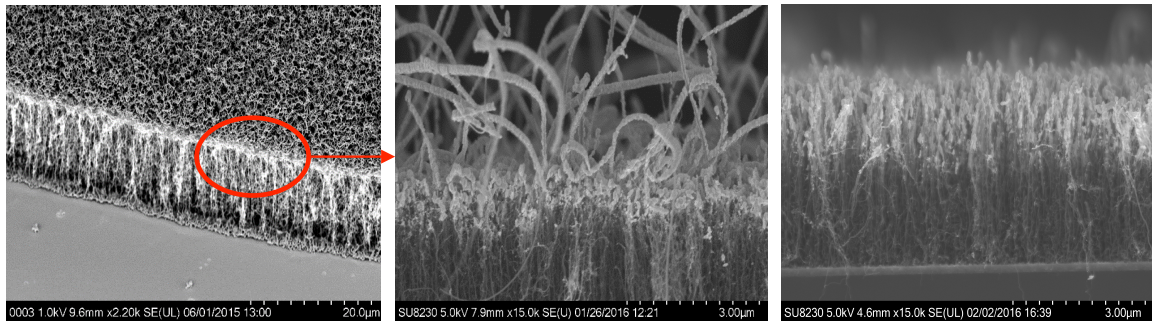


**Figure 3.1.** SEM image of vertically aligned MWCNT film (left) and high magnification cross-section images of 200 nm Au/MWCNT interface, where tubes are dangling above forest (middle), and plasma treated forest (right).

The presence of defects on CNT tips in Figure 3.2(a) confirms the etching, which results in opening the tips. An increase in the number of defects is known to be proportional to plasma power and time [75].

After etching, CNT density decreases, see Figure 3.2(b) which helps in reducing the screening affect in the electric field [75]. CNTs' response to etching time is interesting; after the first 30s the CNT length increases rather than decreasing, see Figure 3.2(c), which is due to straightening /stretching under the plasma bias whereas density is decreased, while after 30s, CNT length and density starts decreasing significantly with

time as seen in Figure 3.2(c, right) [76]. An excessive decrease in CNT density will lead to a lower number density of effective diodes, thus an etch time beyond 30 s is not desirable.

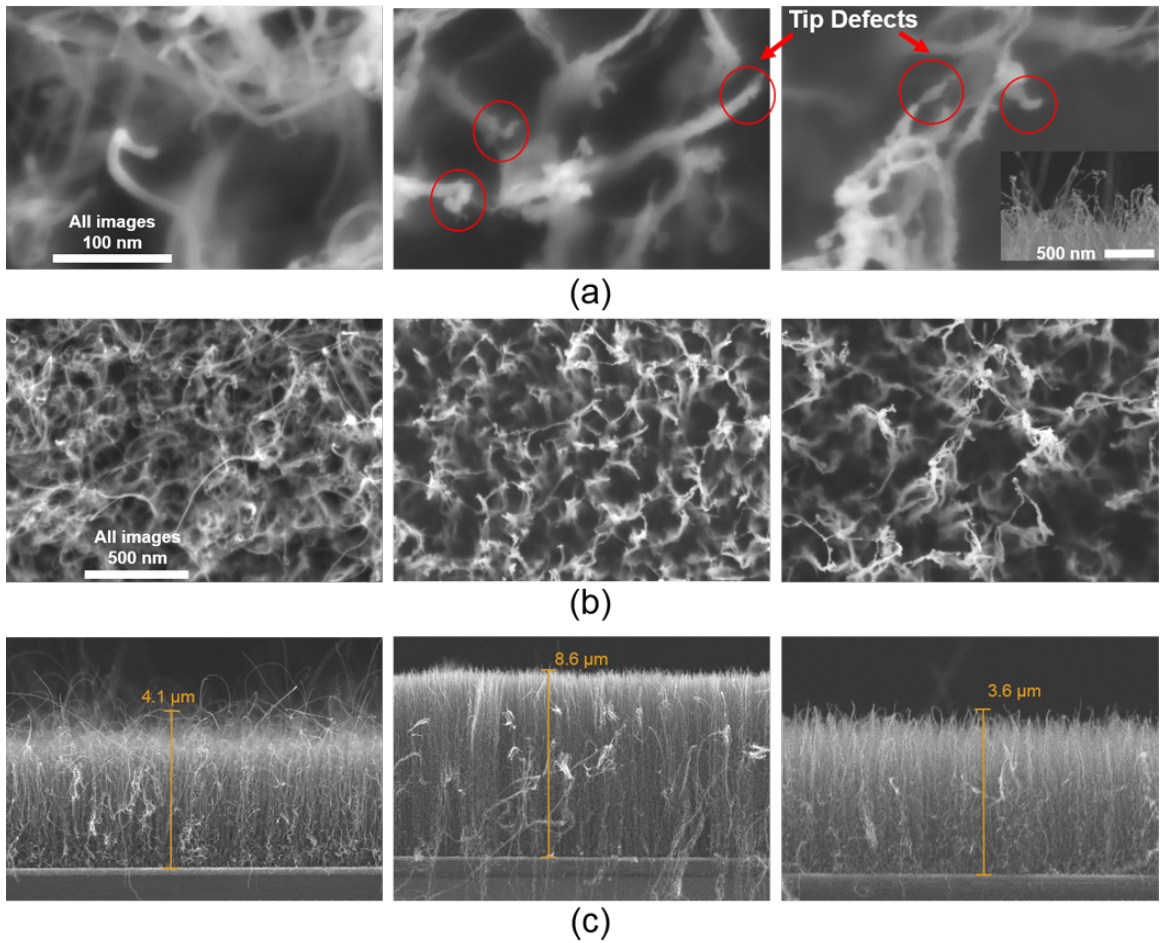


**Figure 3.2.** SEM images of MWCNTs (left) before and (middle) after  $O_2$  plasma etch at 80W for 30s, and (right) 60s at (a) high magnification (b) lower magnification, and (c) lowest magnification with cross-section view.

## 3.2 Phase 2

After selecting best thickness for top metal and plasma conditions for opening CNT tips, experiments conducted in the second phase of this study were designed to examine the complete diodes fabricated with low workfunction Ca (2.83 eV), medium workfunction Al (4.3 eV) and a high workfunction Au (5.1 eV) top metal.

### 3.2.1 Appropriate Thickness for Insulator Layer

In this phase our prime goal was to find the best insulator ( $\text{Al}_2\text{O}_3$ ) thickness for an efficient MWCNT rectenna diode. An insulator typically should be less than 2 nm thick to allow significant electron tunneling and rectification [77]. We deposit thicker oxide because of the possible diffusion of top metal through the thin oxide layer; so 3 nm, 5 nm and 8 nm thick oxide layered devices were tested. It should be noted that a specialized low-energy metal evaporator was used to minimize the penetration distance of metal atoms into the thin oxide insulator.

## **CHAPTER 4**

### **DEVICE FABRICATION**

The major components of our device are MWCNT-Oxide-Metal diode and the antenna. MWCNTs, which are grown for the diode, work as the antenna as well, as in our design the antenna itself as an integral part of the diode. The fabrication process starts with the growth of MWCNTs then oxide layer and metal layer deposition. Below is the detailed description of all the fabrication steps involved for the complete rectenna device.

#### **Step 1: MWCNTs Growth**

CNTs are the main component of the device as they play a dual role of a metal in the diode and as an antenna. For the diode, we need high workfunction metallic CNTs and for the antenna functioning at the visible frequencies, CNTs of specific length and diameter were required. As the resistivity of the substrate also plays a role in the diameter [78] and workfunction of the CNTs we used low resistivity (0.001 – 0.005 Ohm.cm) N-type Si wafer as the substrate for the small diameter CNTs with high workfunction [79]. Catalyst layers of Ti, Al and Fe of thickness 150, 10 and 3 nm were evaporated on Si substrate using e-beam evaporator. A Ti layer works as the adhesive base layer, which keeps the CNT array stick to the substrate, the Al layer helps keep the Fe nanoparticles separated as it makes porous alumina to absorb Fe and Fe layer converts into the nano-islands upon which CNTs grow. Before evaporating catalyst layers, a SiO<sub>2</sub> layer of 200 nm was evaporated on half of the sample to provide probing location away from active device area. Then vertically aligned MWCNTs were grown in an Aixtron Black Magic

reactor using low-pressure chemical vapor deposition (LPCVD). CVD is a controllable growth process for vertically aligned CNTs and it uses hydrocarbon gases as the carbon source [80]. Figure 4.1 is a schematic diagram of the MWCNTs growth process. It has two growth types: tip growth, where the CNT grows while carrying the metal particle to the top of the forest or root growth, where the CNT grows on the metal particle, which stays at the substrate [81].

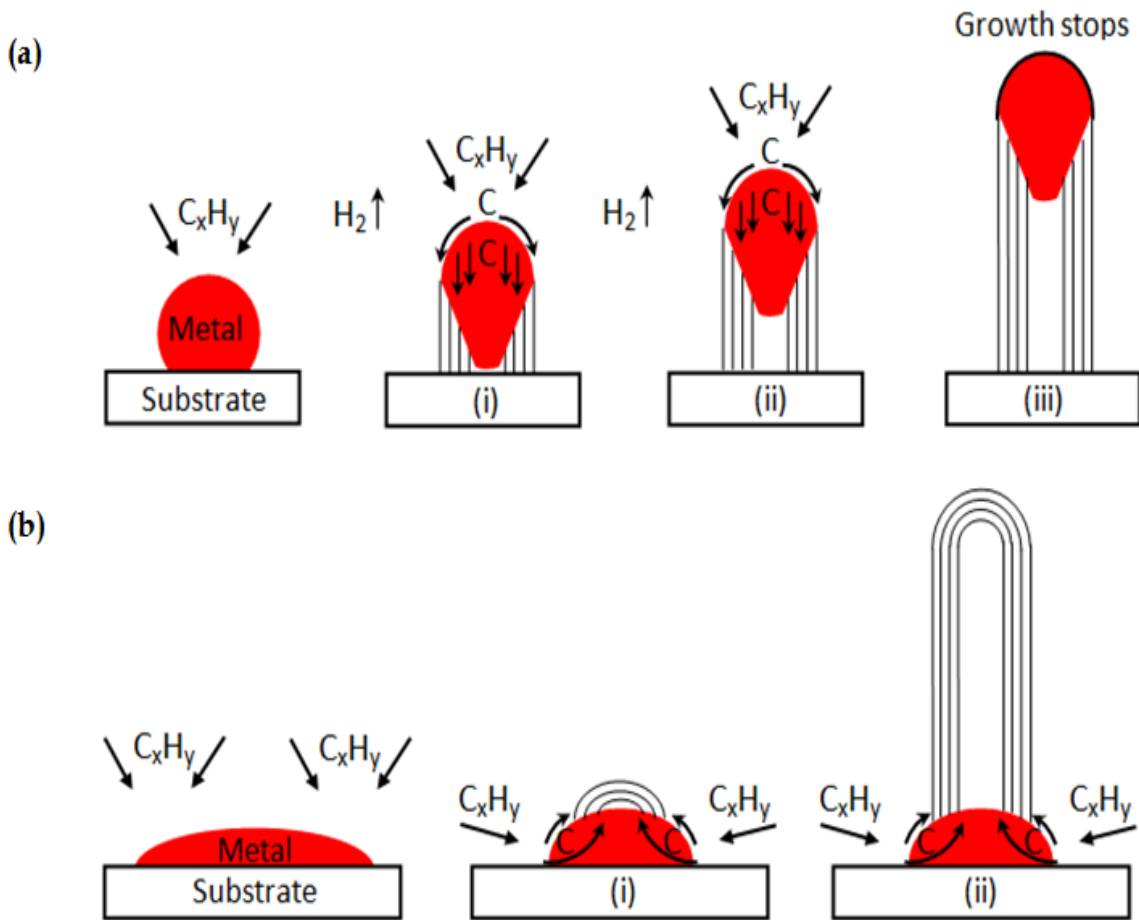


**Figure 4.1.** Multiwall carbon nanotube growth process by chemical vapor deposition, (a) tip growth (b) root growth

Our process is root growth as porous  $Al_2O_3$  and Ti base layers keep the iron particle down at the substrate. Growth begins by decomposing the hydrocarbon and dissolving

the carbon in the hot metal catalyst. Then the metal particle is saturated, and crystallization is initiated, forming cylindrical walls from the carbon to make up the MWCNT [82]. Fe is used as the transition metal, as it is capable of decomposing gas molecules containing a carbon source used for the CNT growth [83, 84]. The growth process was set at 1kPa and 850 °C with C<sub>2</sub>H<sub>2</sub> as the carbon source gas while the growth time was set to be 3 minutes, which gave ~ 8-10 μm long MWCNTs.

Before using the Black Magic reactor, Surrey NanoGrowth system was used to see the impact of different parameters on the CNT growth and the results helped getting the understanding for CNT growth mechanism and the final recipe for the growth.

### **Step 2: Opening CNTs**

CNTs are closed tubes with the hemi-spherical cap covering them on the top. As explained earlier, removing the tips helps improve the bonding of CNTs and reduces the contact resistance with the upper layer. CNT tips were opened by etching them in Unaxis reactive ion etcher (RIE) while using 80 watt oxygen plasma with four etching times of 30, 60, 90 or 120 seconds. Plasma helps removing the dangling CNTs over the forest and straightens them. Figure 4.2 shows the scanning electron microscopy (SEM) of CNTs at different locations of a sample 1 before etching and after etching for 30, 90 and 120 seconds. Similarly does the Figure 4.3 for 60 seconds etching of sample 2. Sample 1 and 2 are grown with same recipe but have variations in CNT length. Characterization under SEM and the Raman spectroscopy is used to confirm the etching and opening of CNTs.

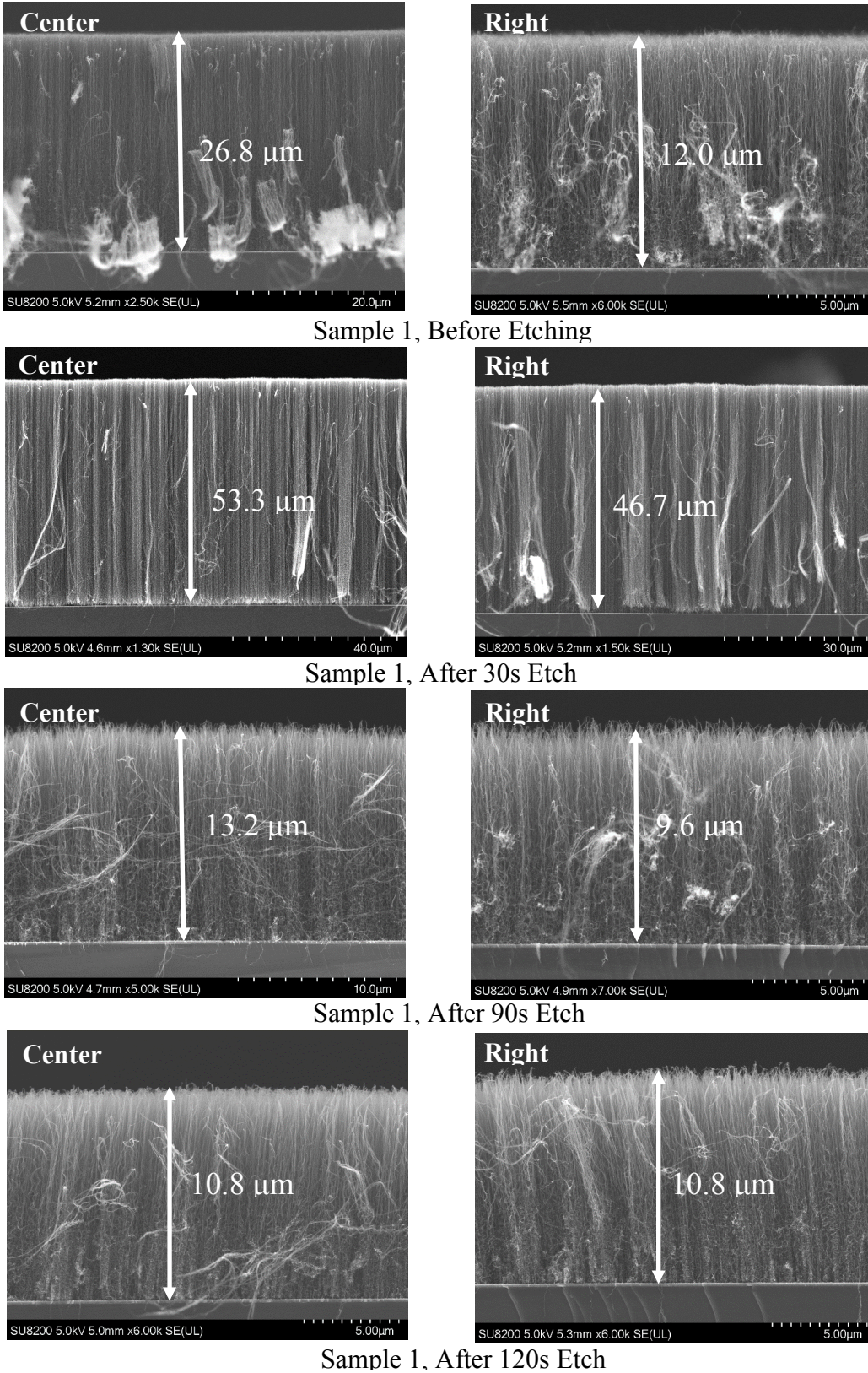
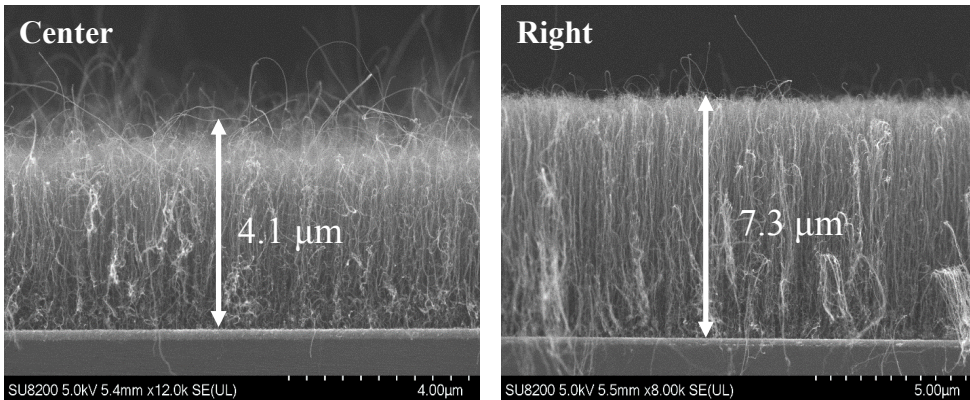


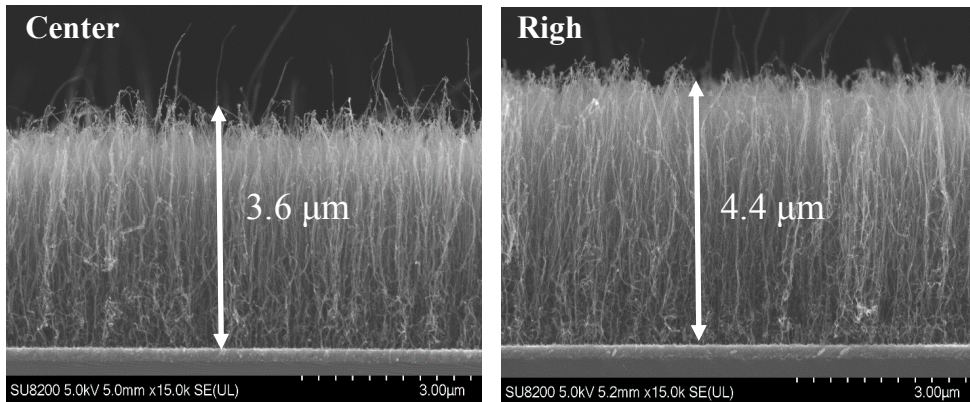
**Figure 4.2.** SEM of sample 1

Sample 1 Analysis:

Before Etching → Avg. Length = 19.04  $\mu\text{m}$   
After 30s Etch: Avg. Length = 50  $\mu\text{m}$ ,  $\Delta L = +30.96 \mu\text{m}$   
After 90s Etch: Avg. Length = 11.4  $\mu\text{m}$ ,  $\Delta L = -7.64 \mu\text{m}$   
After 120s Etch: Avg. Length = 10.8  $\mu\text{m}$ ,  $\Delta L = -8.24 \mu\text{m}$



(Sample 2, Before Etching)



(Sample 2, After 60s Etch)

**Figure 4.3.** SEM of sample 2

Sample 2 Analysis:

Before Etching → Avg. Length = 5.7  $\mu\text{m}$ ;  
After 60s Etch: Avg. Length = 4  $\mu\text{m}$ ,  $\Delta L = -1.7 \mu\text{m}$

From Figure 4.2, it is clear the CNT's length almost doubles up after 30 sec etch [76], while after that length starts decreasing with increasing etch time.

### **Step 3: Oxide Deposition**

Oxide deposition is the most critical part of the fabrication process. Oxide works as the insulator in MIM diode and its thickness defines the rectification. Atomic layer deposition (ALD) is an ideal technique to deposit the ultrathin films of insulator with high conformity and precise control of thickness [85-87]. The deposition is controlled at the atomic level by self-limiting surface reactions. Consequently, uniform and conformal deposition will occur on high aspect ratio porous structures because of self-passivating the surface chemistry. Once the reaction is completed at one surface site, the reactants will continue to travel down the high aspect ratio pore and reach unreacted surface sites.

We used  $\text{Al}_2\text{O}_3$  as the insulator layer.  $\text{Al}_2\text{O}_3$  layers of 3, 5 or 8 nm thicknesses were deposited on open tip MWCNTs by atomic layer deposition (ALD) at 250 °C using trimethylaluminium (TMA) and water ( $\text{H}_2\text{O}$ ) vapors. These thicknesses are based on optimized ALD cycles (100 cycles = 10 nm). Purge times of 30 seconds were used in each ALD cycle for both TMA and  $\text{H}_2\text{O}$  to enable the TMA and  $\text{H}_2\text{O}$  vapor to diffuse completely from the MWNT tips to the substrate base. Between two sets of ALD, oxygen plasma was used to oxidize the surface of the MWCNTs and introduce hydrophilic moieties<sup>16, 17</sup> ( $-\text{OH}$  and  $-\text{COOH}$ ), which promote uniform nucleation and conformal deposition of  $\text{Al}_2\text{O}_3$  on the MWCNTs. Schematics of the whole procedure is shown in Figure 4.4 [88].

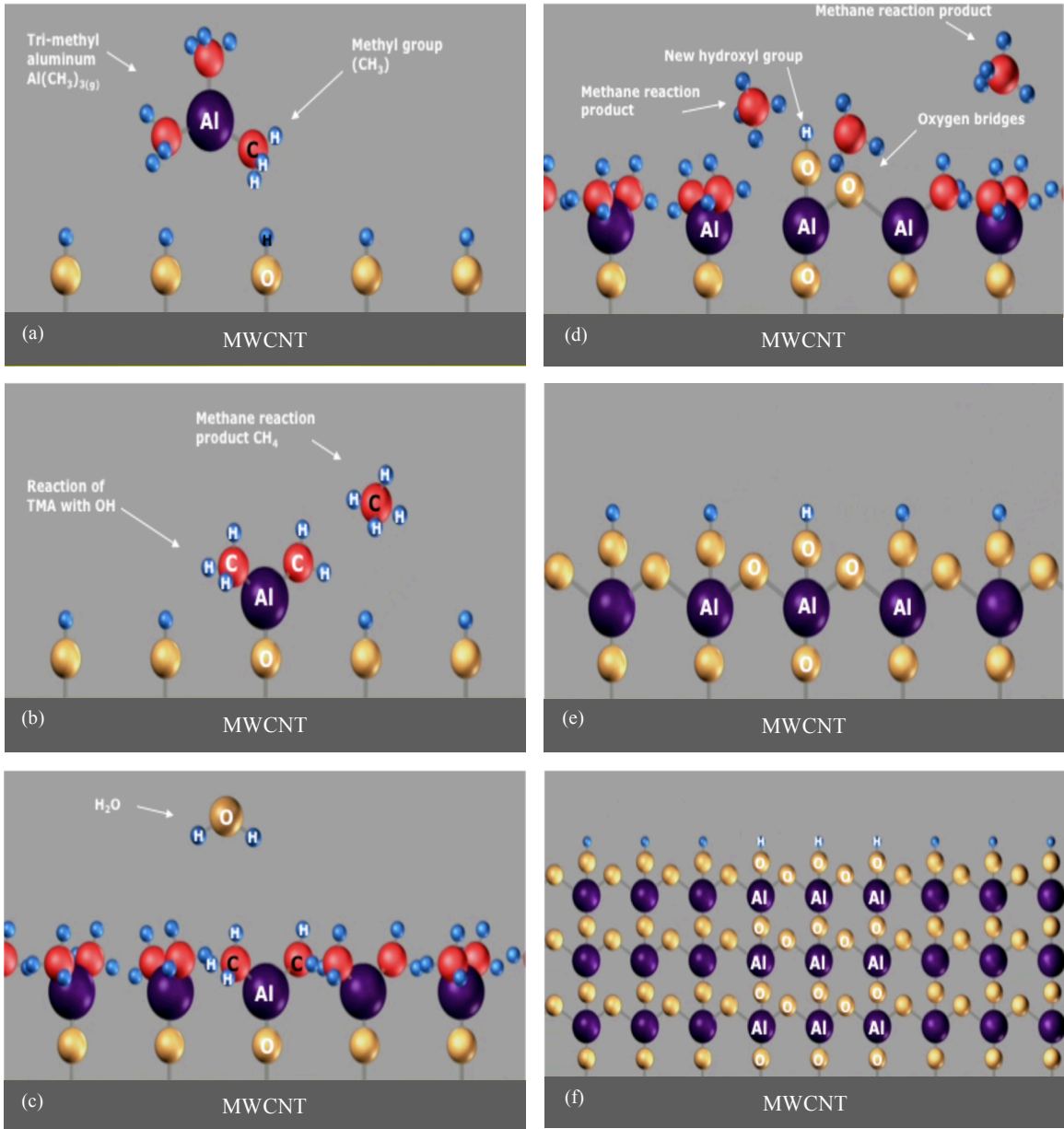


**Figure 4.4.** Step by step demonstration of oxide deposition using Atomic Layer Deposition (ALD)

#### Step 4: Top Metal Deposition

For the first phase of experiments three different thicknesses 50, 200 and 500nm of Ti, Al, Ni and Au were evaporated over CNTs using e-beam evaporator under  $2 \times 10^{-6}$  torr pressure. For the comparison of bonding with open and closed tip CNTs, all of the four metals of all three thicknesses were deposited on open tip CNTs as well. While CNT tips were opened by etching CNTs in Unaxis reactive ion etcher (RIE) using 80 watt oxygen plasma with four etching times of 30, 60, 90 or 120 seconds. After selecting the appropriate thickness of top metal; in the second phase of experiments, three different top metals: Ca, Al and Au of different workfunction were evaporated under vacuum pressure (base pressure less than  $10^{-7}$  torr) using a specialized low energy and long working distance e-beam evaporator so that metal doesn't penetrate through the thin oxide layer. Ca 50nm capped with 60 nm Al and 90 nm Ag; 60nm Al capped with 150nm Ag and 200 nm Au were exact compositions of three metal depositions. Ag coating was used to prevent or minimize oxidation of Ca, Al in air. The source metals were from Lesker and had a purity of 99% or greater. Figure 4.5 shows the metal layer covering the MWCNTs.

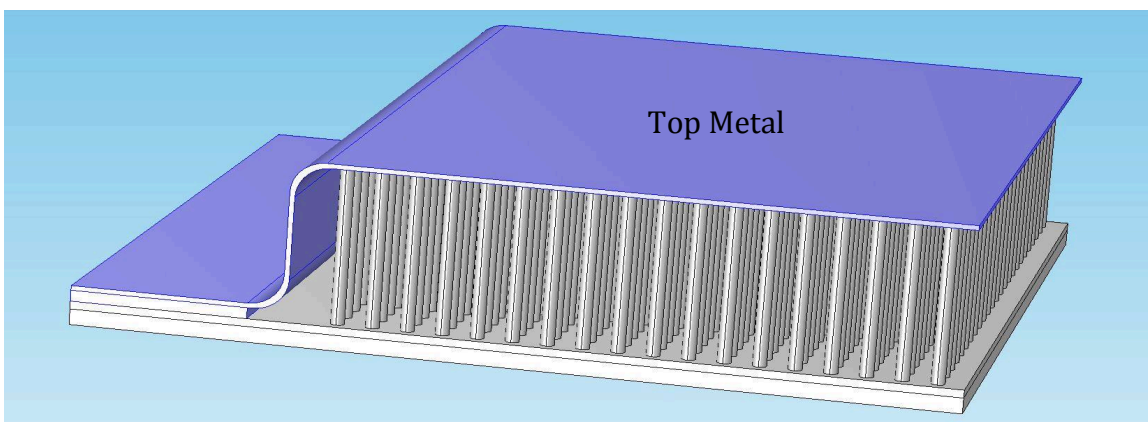


**Figure 4.5.** Top metal blanket over the MWCNTs

### Pictorial Summary of Fabrication Process

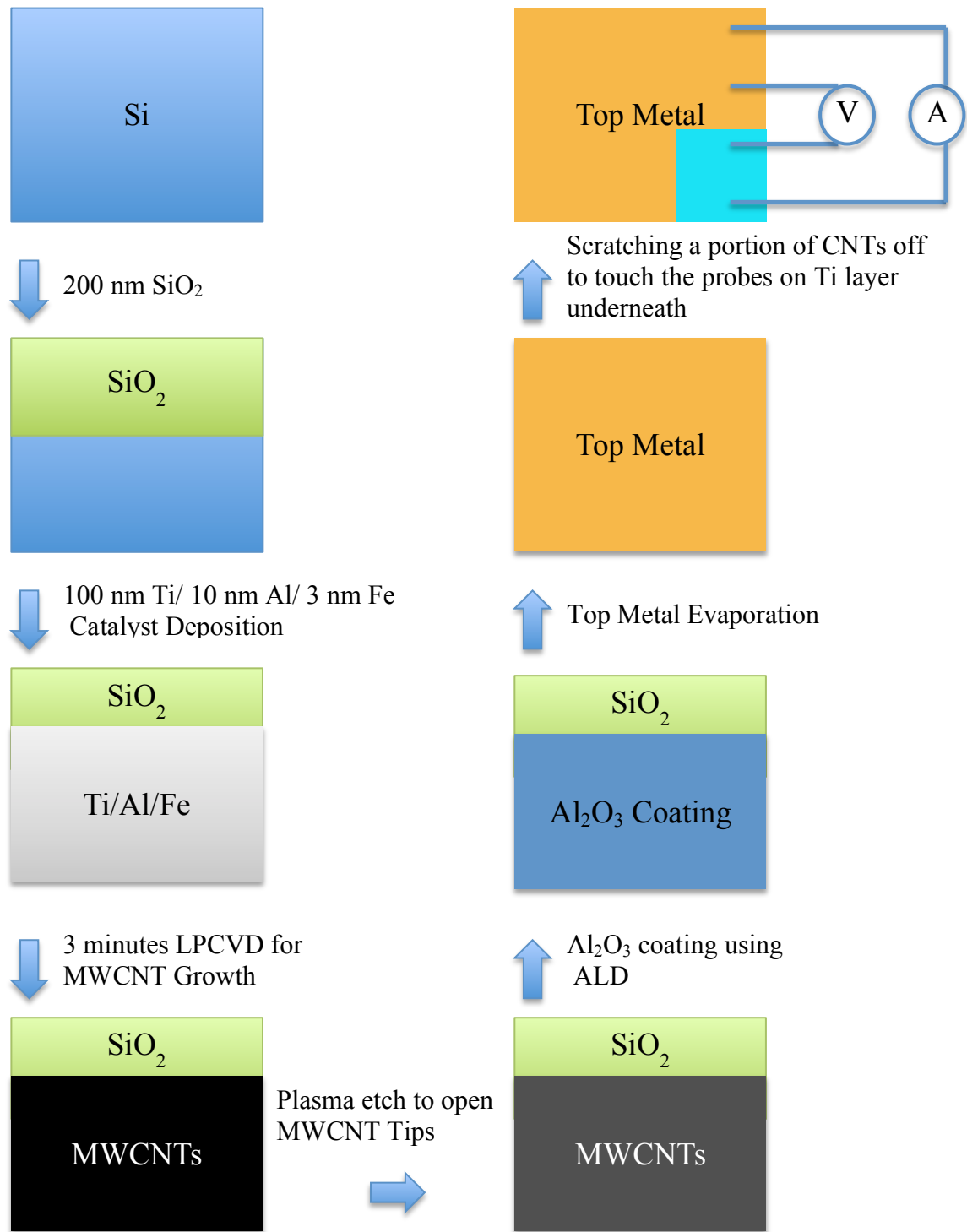


**Figure 4.6.** Block diagram of complete fabrication process of MWCNT-Al<sub>2</sub>O<sub>3</sub>-Metal rectenna over 1X1 inch substrate

## **CHAPTER 5**

### **DEVICE CHARACTERIZATION**

#### **5.1 Scanning Electron Microscopy**

Scanning Electron Microscopy (SEM) produces an image of the sample by scanning it with the focus beam of high-energy electrons. The signals produced by the electron-sample interaction reveal the information about sample morphology, chemical composition and crystalline structure [89]. We have used Hitachi's next generation Cold Field Emission SU8230 SEM, which offers unmatched low-voltage imaging and comprehensive analytical microanalysis. In our work, SEM was mainly used to characterize MWCNTs grown over Si substrate. One out of every three similar samples was characterized. Samples were characterized at different magnifications, ranging from 1k to 100k to see the growth pattern and to measure the dimensions of discrete MWCNT. SEM played a vital role in identifying the opening of CNT tips after plasma etching. Defects on MWCNT tips (Figure 3.2) and their length reduction (Figure 4.2, 4.3) after plasma etching confirmed the opening of MWCNT tips, which was one of the main goals in this study. The second major contribution of SEM was showing the conformity of top metal deposition on the MWCNTs. Three different thicknesses (50 nm, 200 nm and 500 nm) of each of four different metals (Ti, Ni, Al, Au) were deposited. SEM images helped in identifying average thickness of top metal. While looking at the conformity of metal deposition over the CNTs, it can be seen in the SEM scans in Figure 5.1 that Ti had the most conformal layer while Au has poor conformity as it deposited in the forms of beads which clearly shows the Ti has better wetting with CNTs.

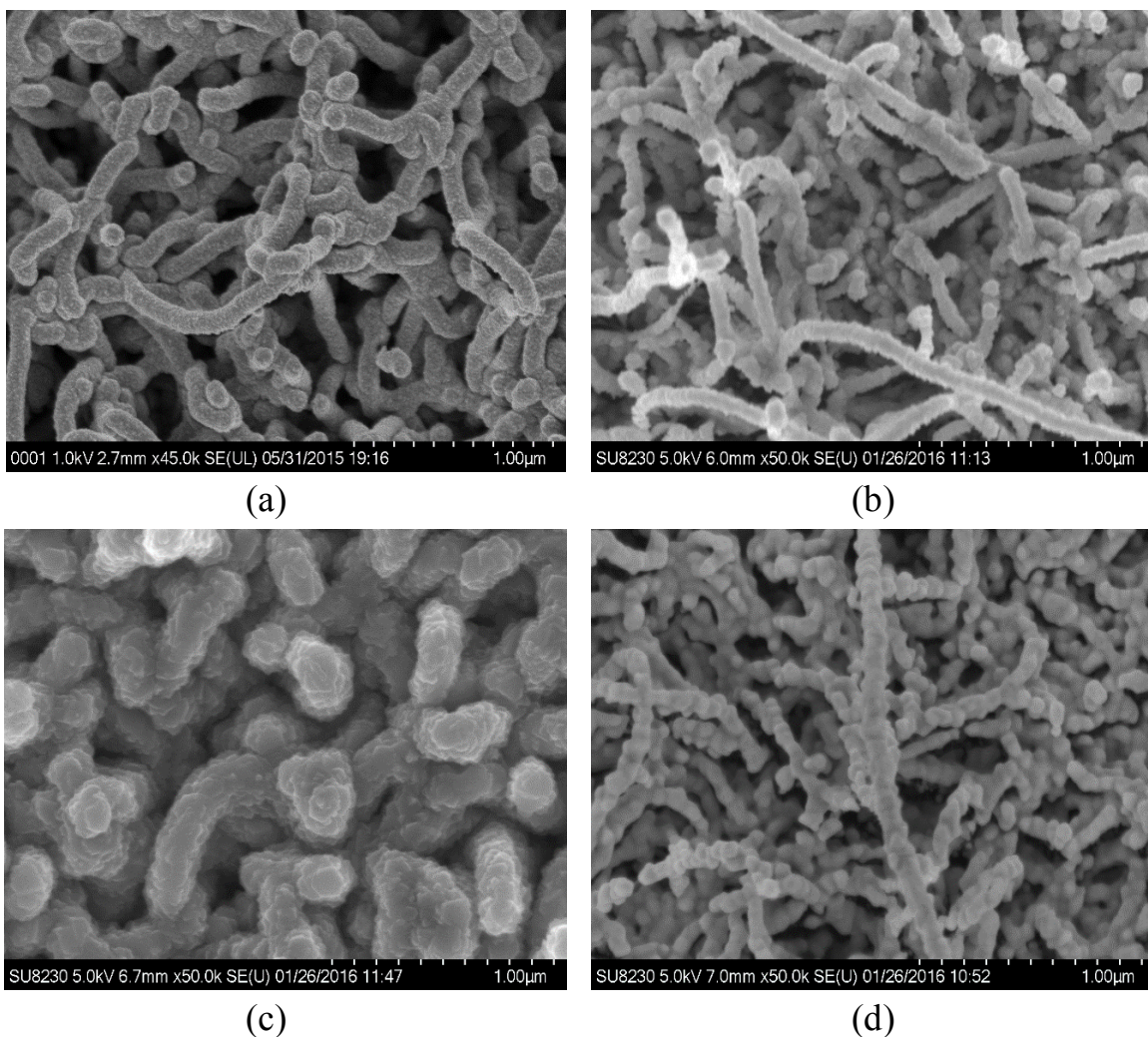


**Figure 5.1.** Top down SEM images of (a) 200 nm Ti, (b) 200 nm Ni, (c) 200 nm Al and (d) 200 nm Au coated closed tip MWCNTs.

## 5.2 Raman Spectroscopy

Raman spectra in Figure 5.2 show a relatively high  $I_G/I_D$  peak intensity ratio of 1.17 for the as-grown CNT forest, whereas the  $I_G/I_D$  ratio decreases significantly to 0.98 after the 30 s plasma etch. Continuing to etch the CNTs for an additional minute further decreased the  $I_G/I_D$  ratio to 0.90. This data confirmed that the surface region of the CNT forest was

etched thereby creating a substantial amount of defects, such as dangling bonds at open CNT tips, during the first 30 seconds of etch time.

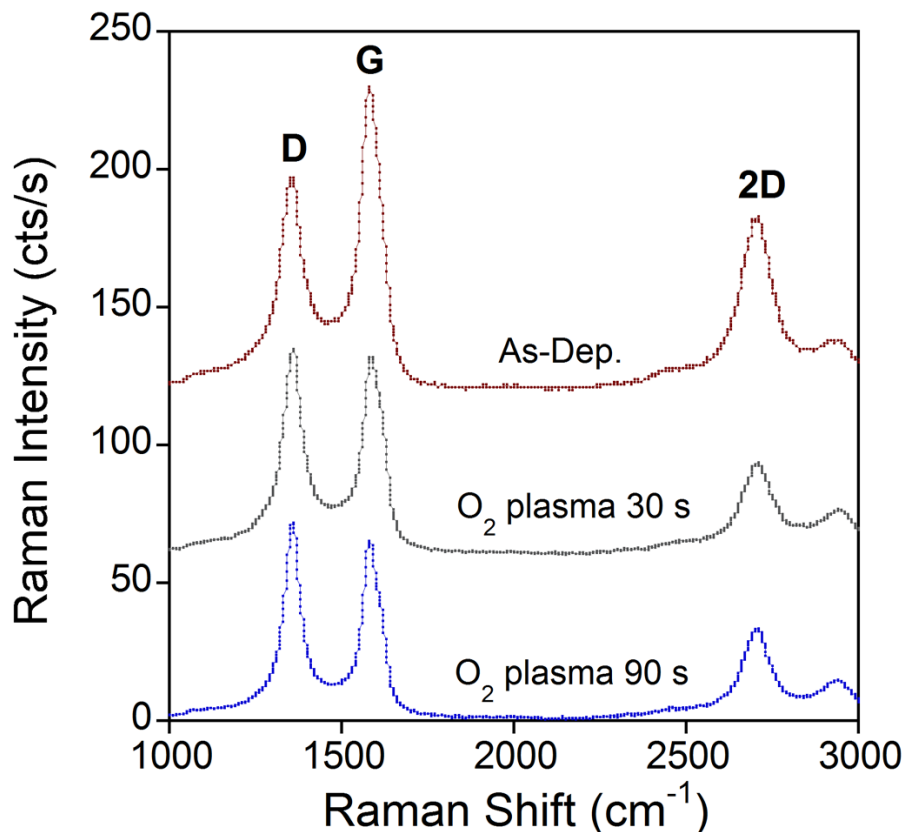


**Figure 5.2.** Effects of oxygen plasma etch on Raman  $I_G/I_D$  ratio: as-deposited MWCNTs (red curve), after 80 W plasma etch for 30 seconds (black curve) and 90 seconds (blue curve).

Raman spectroscopy measurements (Figure 5.2) with incident laser wavelength of 488 nm were also used to gain further insight on the effect of the oxygen plasma treatment. Typical for sp<sup>2</sup>- hybridized carbon samples, including CNTs, the long range ordering of the hexagonal graphite lattice or conversely the proportion of disorder and defects can be characterized by observing the intensity ratios of the Raman D and G bands. The Raman D band around 1350 cm<sup>-1</sup> corresponds to disordered and defective graphitic carbon

whereas the G band around  $1580\text{ cm}^{-1}$  corresponds to highly ordered graphitic carbon. Figure 5.2 confirmed that although CNT length may have increased due to improved CNT alignment in the plasma environment, the surface region of the CNT forest was still etched thereby creating a substantial amount of defects, such as dangling bonds at open CNT tips, during the first 30 seconds of etch time.

### 5.3 I-V Characterization

The current – voltage (I-V) measurements of the devices were done using an Agilent E5272A source monitor unit connected to a DC electrical 4-probe station with a temperature-controlled stage. The resistance of the tungsten probe and lead wires was on the order of  $1\ \Omega$ . A 4-probe is preferred over a traditional 2-probe system because of its higher accuracy and also for the sheet resistance measurements [90]. Current (I) was forced in through two outer probes and voltage (V) was sensed on the inside probes. All the four probes were kept apart at equal distances in-between. Figure 5.3 shows the placement of probes across the sample. All the contact and sheet resistances were measured to see the role of each resistance in the total diode resistance. Firstly sheet resistance of Ti layer was measured. For that all the 4-probes were kept on the Ti layer with equal spacing. Then to see the impact of top metal thickness, resistances of devices with all three thicknesses i.e. 50nm, 200nm, 500nm of each of four metals (Ti, Al, Ni, Au) were measured. Next, to find the exact contact resistance of MWCNT-Top Metal, sheet resistances of all the 4 metals were measured. To see the impact of opening the CNT tips on overall resistance, open-tip and closed-tip device resistances were measured. Similarly in Phase 2 of experiments the impact of different thicknesses on insulator layer

was observed. A key factor during the I-V characterizations was the adjustment of probes. Initially, Cu-tape was used as an intermediate between probe and the sample but it added resistance because of the glue on the tape. So to maintain accuracy, the probes were directly placed on the top of metal layers while making sure through the microscope that probes were not poking through the upper metal layer to touch directly MWCNTs. In our electrical probe setting current flows from the probe to the top metal and insulator (MWCNTs are coated with  $\text{Al}_2\text{O}_3$ ) and then via MWCNTs it goes to Ti layer where it is sensed.  $\text{SiO}_2$  layer over the Si substrate insulates the current path to Si wafer and routes it to top-metal.

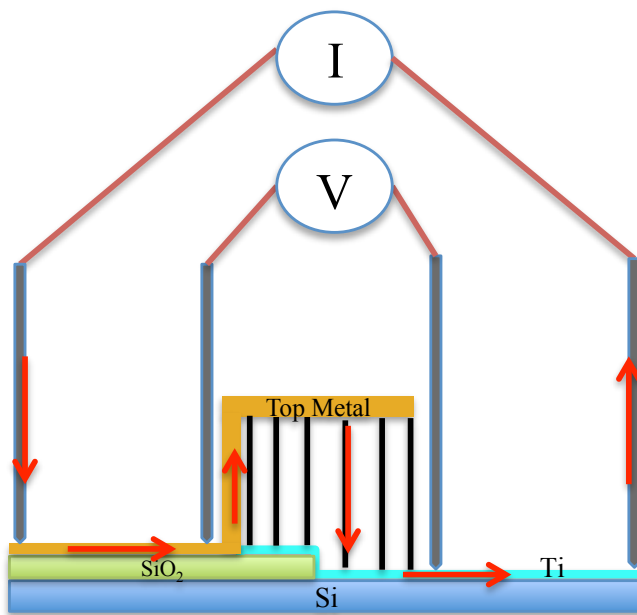


**Figure 5.3.** Schematics of 4-probe resistivity measurement system (red arrows show the flow of current)

## CHAPTER 6

### RESULTS AND DISCUSSION

#### 6.1 Phase 1

##### 6.1.1 Influence of Top Metal Thickness on Contact Resistance

We studied MWCNT interface resistance in Phase 1 of the study. To study the impact of top-metal thickness, we have tested 3 different thicknesses (50nm, 200nm and 500nm) on four different metals i.e. Ti, Al, Ni and Au. So that before defining the final thickness of top-metal we have enough sample size. While looking at the electrical characteristics in Figure 6.1, it can be inferred that Ti with lower work function (4.4 eV) has a lower resistance than Au (5.1 eV) and Ni (5.04 eV). The lower resistance is likely related to TiC formation at the interface, which provides better wetting or adhesion thereby reducing the MWCNT-Ti contact resistance [91]. Instead of a uniformly coated contact region like Ti, the deposited Au formed nanoclusters that cover the CNT surface discretely (Figure 5.1). The atomic vacuum gap results in a large series contact resistance or a physical barrier [92]. In the case of Al, which also has a lower workfunction i.e. 4.06 eV it showed higher resistance and some non-linearity, which could be due to potential oxidation of Al to form insulator ( $\text{Al}_2\text{O}_3$ ) layer between CNT and Al. These results clearly indicate that the electrical contact resistance with MWCNT is not determined by the barrier height but correlates to the cohesive strength of the electrode-carbon interface attributed to better wettability of metal [91].

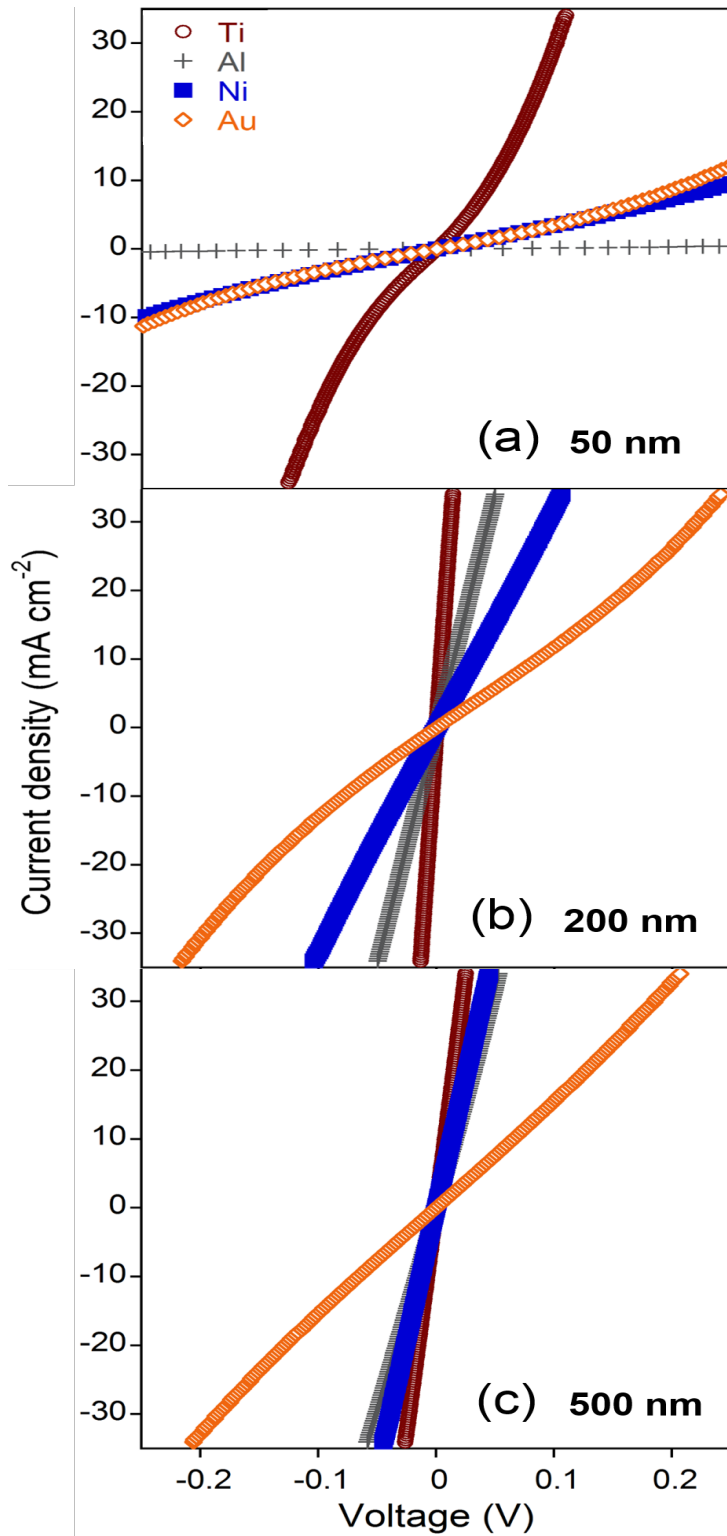


**Figure 6.1.** Influence of the choice of top metals (Ti, Al, Ni and Au) and their thickness on I-V characteristics: I-V plots for (a) 50 nm, (b) 200 nm, and (c) 500 nm top metal thickness samples.

For different thicknesses of top metals, 50 nm has shown the highest resistance, whereas 200 and 500 nm films have shown the lower resistances (Figure 6.2). This is because as the film thickness increases the grain size increases [93] and increasing grain size decreases the resistance due to grain- boundary scattering as well as to the Fuchs size-effect [94]. For exact values of average resistance, please refer to Table A.1 in appendix. Finally, we decided 200 nm to be a sufficient thickness to ensure high conductivity of the top metal while reducing processing time and cost compared to a thicker deposition.

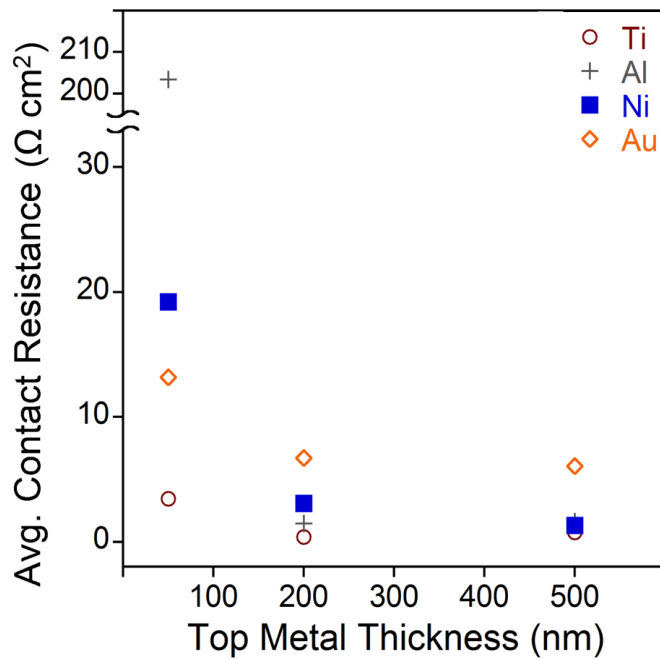


**Figure 6.2.** Plot of average contact resistance for various top metal thicknesses.

### 6.1.2 Sheet Resistance vs. Contact Resistance of Top Metal

I-V curves for sheet resistance measured using 4-point probe method are shown in Figure 6.3. As expected, the trend for sheet resistance is nearly opposite to the trend for contact resistance for the four metal over-layers. The sheet resistance is proportional to the

resistivity of the metals, which is an intrinsic electrical property of the metal [95]. The Au film has the lowest sheet resistance and it is the metal with the highest intrinsic conductivity, whereas the Ti film has the highest sheet resistance and it is the metal with the lowest intrinsic conductivity. Figures 6.1 and 6.2 showed that the Ti-MWCNT contact resistance was much lower than the Au-MWCNT contact resistance and this is attributed to the superior wetting/adhesion property of Ti; in this case the stronger bonding affinity of Ti to the carbon atoms in the MWCNTs.

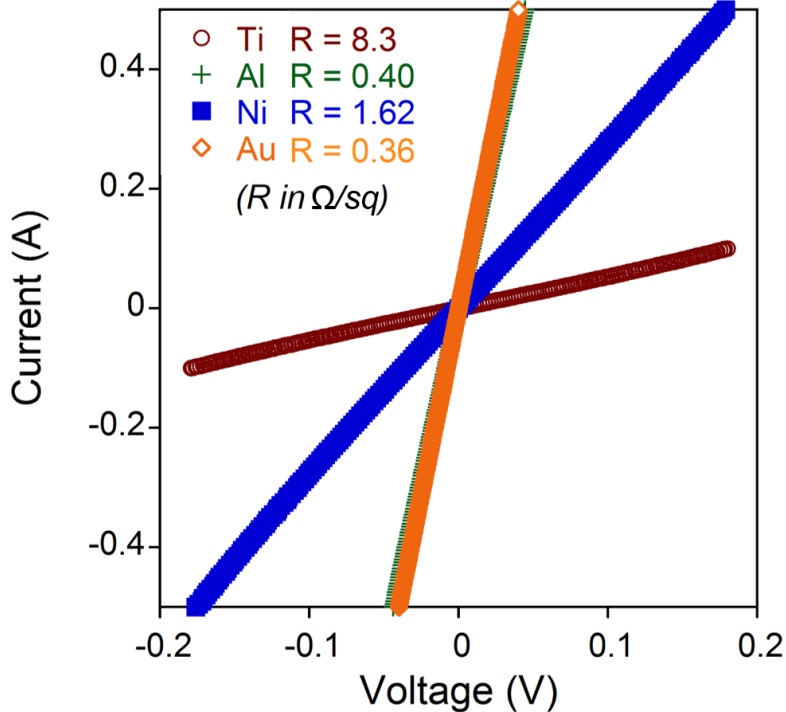


**Figure 6.3.** Four-point probe IV curves showing sheet resistance of top metals (200 nm Ti, Al, Ni and Au).

### 6.1.3 Influence of opening CNT Tips on Contact Resistance

MWCNTs are the main component of our Rectenna device. MWCNT works as a metal of the diode and as an antenna itself. For better coupling of diode and antenna, MWCNT interface is critical to be observed. While looking at the possibilities of reducing overall

resistance, we found that opening MWCNT tips helps increasing metal wettability and results in better bonding with lesser contact resistance. Thus MWCNT tips were removed using plasma etching. Then the contact resistances of all four metals, each of 200nm thickness (Ti, Al, Ni, Au) with opened and closed CNT tips were compared to examine the impact of opening CNTs. All contacts (except Al) showed a slight reduction in resistance (Figure 6.4), thus opening CNT tips has improved bonding and wettability [22].

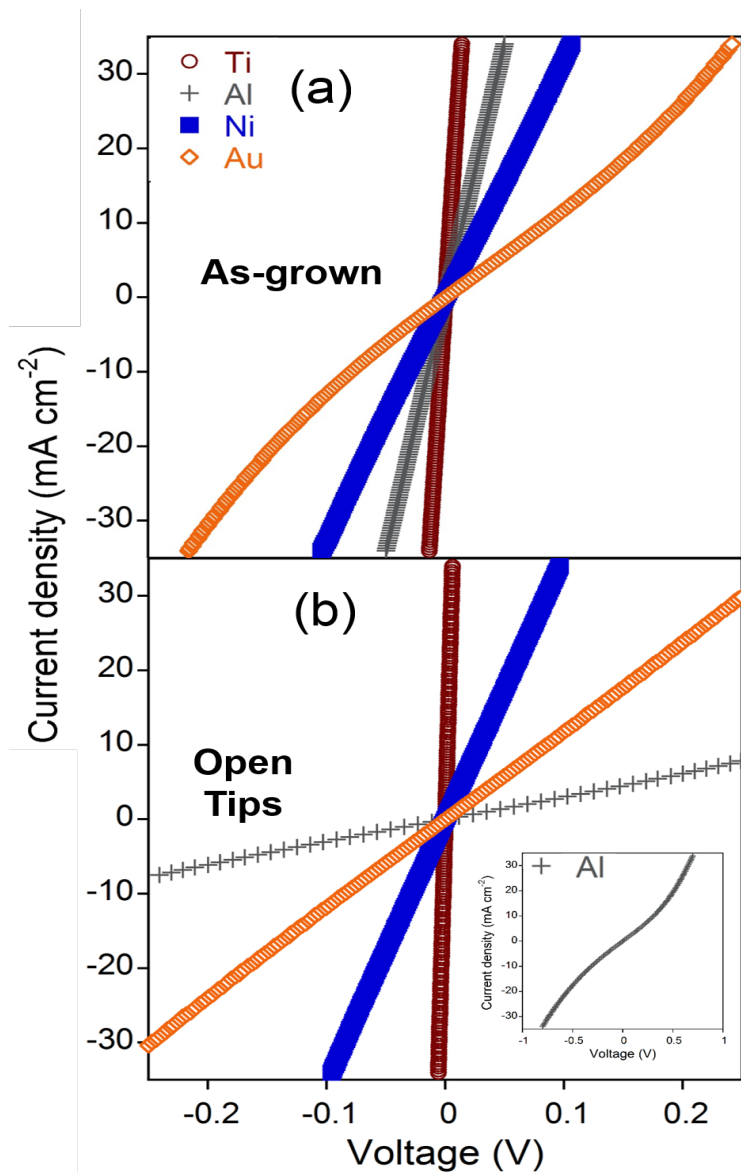


**Figure 6.4.** I-V plots of (a) closed and (b) open tip MWCNTs with 200 nm top metal thicknesses. Inset shows I-V curve with expanded voltage range for Al top metal that exhibits significant non-linearity.

Contrary to other metals, Al has shown a significant increase in resistance and non-linearity in I-V response, see inset of Figure 6.4 (b), which is likely caused by quick oxidation, as Al is the least resistant to oxidation of all the metals considered.

Figure 6.5 shows the percentage change in contact resistance after opening CNT tips to clearly see the impact of opening CNTs. Refer to Table A.2 in appendix for the exact values of resistance change. From these results, it is evident that 200 nm top metal thicknesses with open CNT tips is the best combination for lower contact resistance.

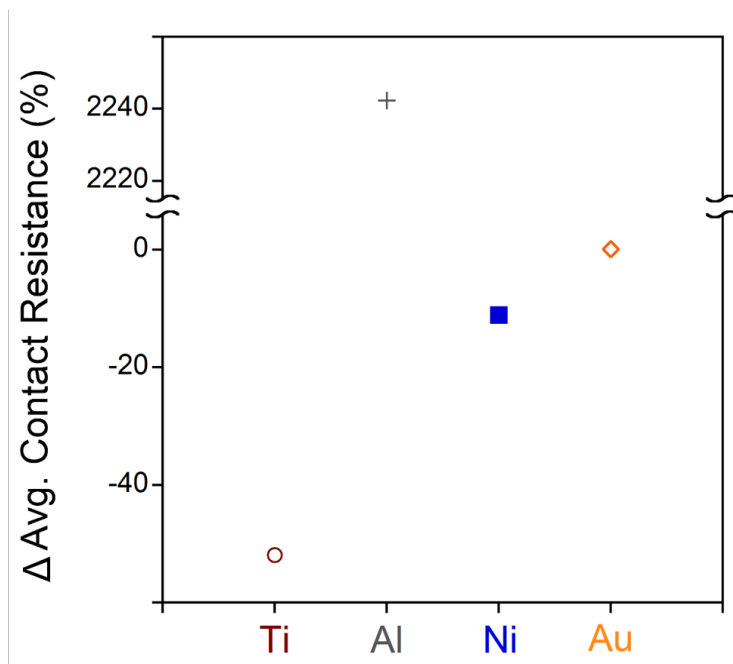


**Figure 6.5.** Percentage change in average contact resistance after opening CNT tips for all four top metals (Ti, Al, Ni, Au) each of 200 nm thickness.

## 6.2 Phase 2

After deciding the top metal thickness and CNT tip morphology, the second phase of the study was to see the role of insulator thickness in over all resistance of MWCNT-Insulator-Metal (MWCNT-I-M) diode. Insulator thickness is very critical to the functionality of the optical rectenna as it affects the specific capacitance and ultimately cut-off frequency. In this phase of experiments Ti, Al, Ni, Au top metals have been replaced with new combinations of metals with low workfunction to maintain the workfunction difference between MWCNT and top metal for rectification.

### 6.2.1 Influence of Insulator Thickness

To identify the ideal thickness of insulator layer in MWCNT-I-M diode, the complete rectenna device structure was analyzed incorporating lower resistance combinations obtained earlier i.e. 200 nm total metal over open ended MWCNTs. Figure 6.6 shows the I-V characterization of three MWCNT-I-M diodes with different oxide thicknesses (3nm, 5nm, 8nm) and three different metals (Ca/Al, Al, Au) top metals for each thickness. Then the resistance plots are generated from the IV characteristics by fitting the sixth-order polynomials (Appendix B) to the measured data. The first derivative of the polynomial gives the differential resistance (R).

$$R = \left(\frac{dV}{dI}\right) \quad (1)$$

It can be inferred from resistance plot (Figure 6.7) that diode resistance increased with oxide thickness for all three different devices.

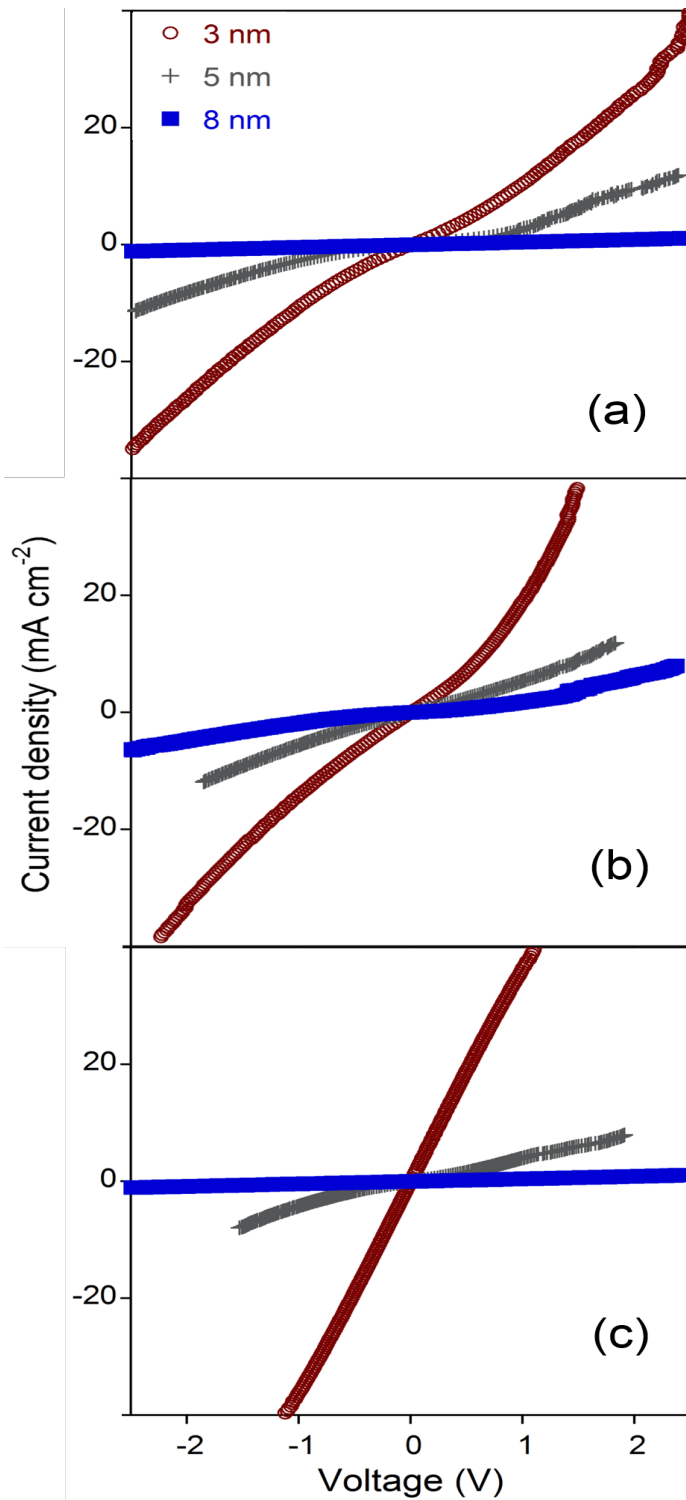


**Figure 6.6.** Influence of oxide thickness and top metal workfunction on I-V characteristics of MWCNT-I-M diodes: Diodes have (a) 50nm Ca / 60 nm Al / 90 nm Ag, (b) 60 nm Al / 90 nm Ag, and (c) 200 nm Au top metal layers. (90 nm Ag layer is just the filling layer to reach the optimized thickness).

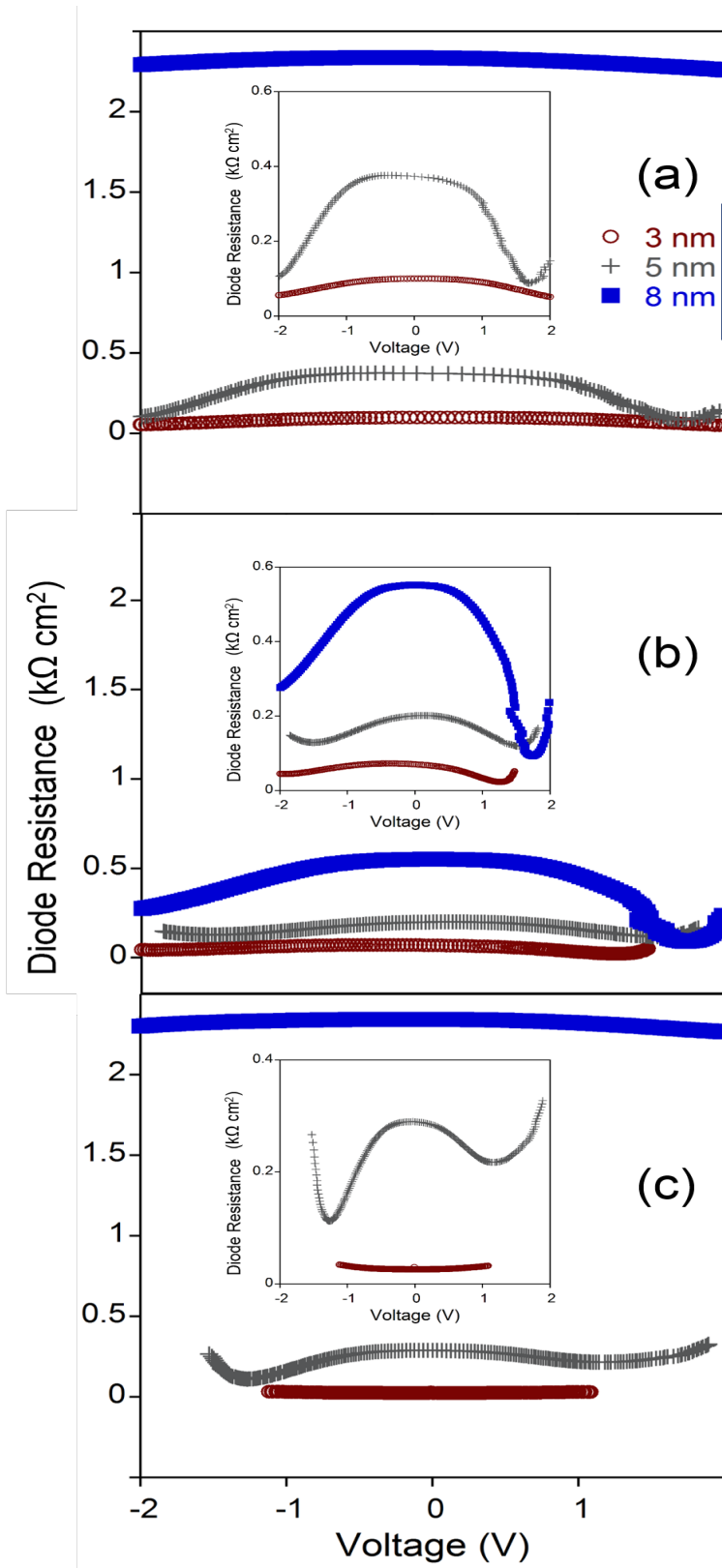


**Figure 6.7.** Diode resistance vs. voltage for devices with: (a) 50 nm Ca / 60 nm Al / 90 nm Ag, (b) 60 nm Al / 90 nm Ag, and (c) 200 nm Au top metal layers. (Insets are zoomed in)

Electron tunneling occurs through 8-10 nm diameter CNT tips thus this smaller diode area leads to very small capacitance and high cutoff frequency. The estimated frequency of operation of a MIM diode can be calculated by determining the capacitance of the diode. The capacitance, with the cutoff frequency being inversely proportional to  $C_D$  of the thin film can be considered as a parallel-plate capacitor.

$$C_D = \frac{\epsilon\epsilon_0 A}{d} \quad (2)$$

Where

$C_D$  is the capacitance

$\epsilon$  is the di-electric constant of insulator ( $\text{Al}_2\text{O}_3$ )

$\epsilon_0$  is the permittivity of free space ( $\epsilon_0 \approx 8.854 \times 10^{-12}$  F/m)

$A$  is the cross-sectional area of the diode; and

$d$  is the insulator thickness

For a 5 nm oxide diode the specific capacitance is  $5.4 \mu\text{F}/\text{cm}^2$  while considering relative permittivity for  $\text{Al}_2\text{O}_3$  deposited through ALD in this range of thickness i.e.  $\sim 3\text{-}8$  nm is 3.8 [7], [96]. This results in 2.72 aF capacitance per MWCNT junction as number density of MWCNTs is almost  $10^{10}$  CNTs per  $\text{cm}^2$ . For higher cutoff frequency, we can consider reducing capacitance by thicker oxide; e.g. for 8 nm oxide, capacitance reduces to 1.7 aF but this is not a viable option as the non-linearity of the I-V curve of the diode, and the probability of the tunneling decreases considerably if thickness of the insulator is increased beyond 5nm [97].

Barrier height and width are decisive factors in tunneling probability. The tunneling probability of the particle is established by the barrier height and width. The transmission probability is given by the modified Schrödinger Wave equation,

$$D = e^{(-2d \sqrt{\frac{2m(V-E)}{\hbar^2}})} \quad (3)$$

Here, V is the barrier height and E is the energy of the particle. D is the transmission probability and d is the thickness of the insulator. For a particle with a mass of an electron, the tunneling probabilities for  $d=1\text{Å}$ ,  $10\text{ Å}$  and  $100\text{ Å}$  are 0.68, 0.02 and  $3 \times 10^{-17}$ , respectively. So an electron can tunnel through a barrier with distance in atomic range. However, once the distance gets increased more than atomic dimensions, the tunneling probability decreases [98].

Now that we have diode capacitance, cutoff frequency can be deduced from the following relation:

$$f_c = \frac{1}{2\pi R_A C_D} \quad (4)$$

From the deduced diode capacitance (2.72 aF) for 5nm oxide thickness and MWCNT antenna resistance,  $R_A$  (100  $\Omega$ ) [54], [99], it can be inferred that our device can operate in the visible range at 585 THz frequencies.

## CHAPTER 7

### RECTIFICATION PARAMETERS OF DIODE

To determine the rectification of this MWCNT-I-M diode; zero-bias resistance, responsivity, and asymmetry are three important parameters [8].

#### 7.1 Zero-Bias Resistance

The differential resistance is used to generate resistance versus voltage plots (Figure 6.7).

The important parameter of interest, zero-bias resistance ( $R^{ZB}$ ) is evaluated from this data at zero voltage (Figure 7.1). For exact values, refer to Table A.3 in appendix.

$$R^{ZB} = \left( \frac{dV}{dI} \right)_{V=0} \quad (1)$$

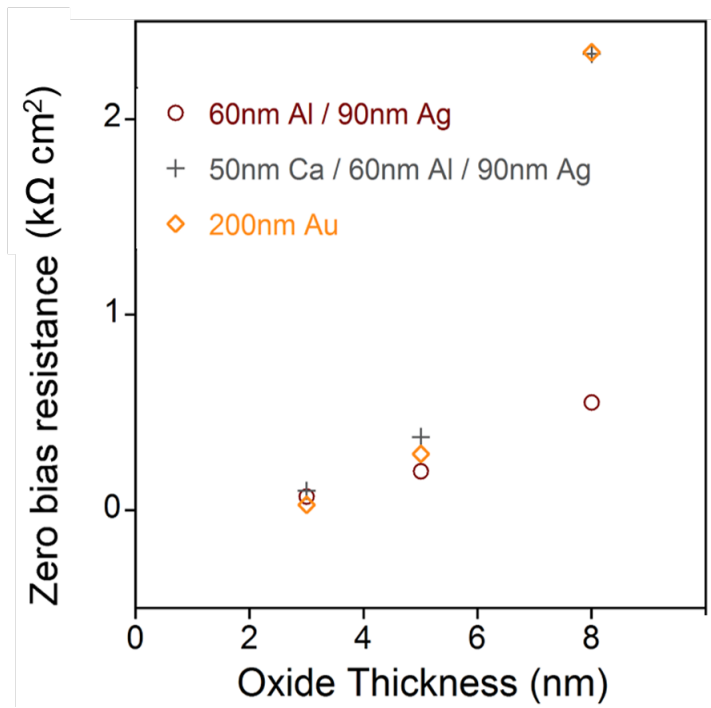


**Figure 7.1.** Effect of oxide thickness on zero-bias resistance of diodes

From the zero-bias plots it is inferred that Au and Al based diodes have lesser resistance which is because of lower workfunction difference from the MWCNTs. While Ca based diode has somewhat higher resistance, which is owed to higher work function difference with MWCNTs. While looking at the oxide thickness, 3nm thick oxide based diodes have the lowest zero-bias resistance, while it increases with the thickness. But diode performance isn't dependent on zero-bias resistance only. Some diodes may have the least resistance but they won't be rectifying electromagnetics waves at all because of poor responsivity and asymmetry. The importance of these factors is elaborated below.

## 7.2 Responsivity

For an efficient rectenna, the diode needs to be fabricated with strong non-linearity to obtain detectors with large response. Hence, the second derivative, which is a standard measure of non-linearity of the diode, is determined [100]. Together with first and second derivative, the sensitivity of the diode is obtained which characterizes the performance of the diode [101]. In simple terms, sensitivity is a measure of the rectified dc voltage or current as a function of input radiant power. However, junction resistance should be low to provide good impedance matching between the antenna and the diode. Responsivity has been calculated using the 6<sup>th</sup>-order polynomial fitted to the I-V characteristic curves of the devices (Appendix B). It is deduced as half the ratio of the second and first derivative of the I-V characteristics [102]. Responsivity is also called sensitivity (S).

$$S = 1/2 \left( \frac{d^2I/d^2V}{dI/dV} \right) \quad (2)$$

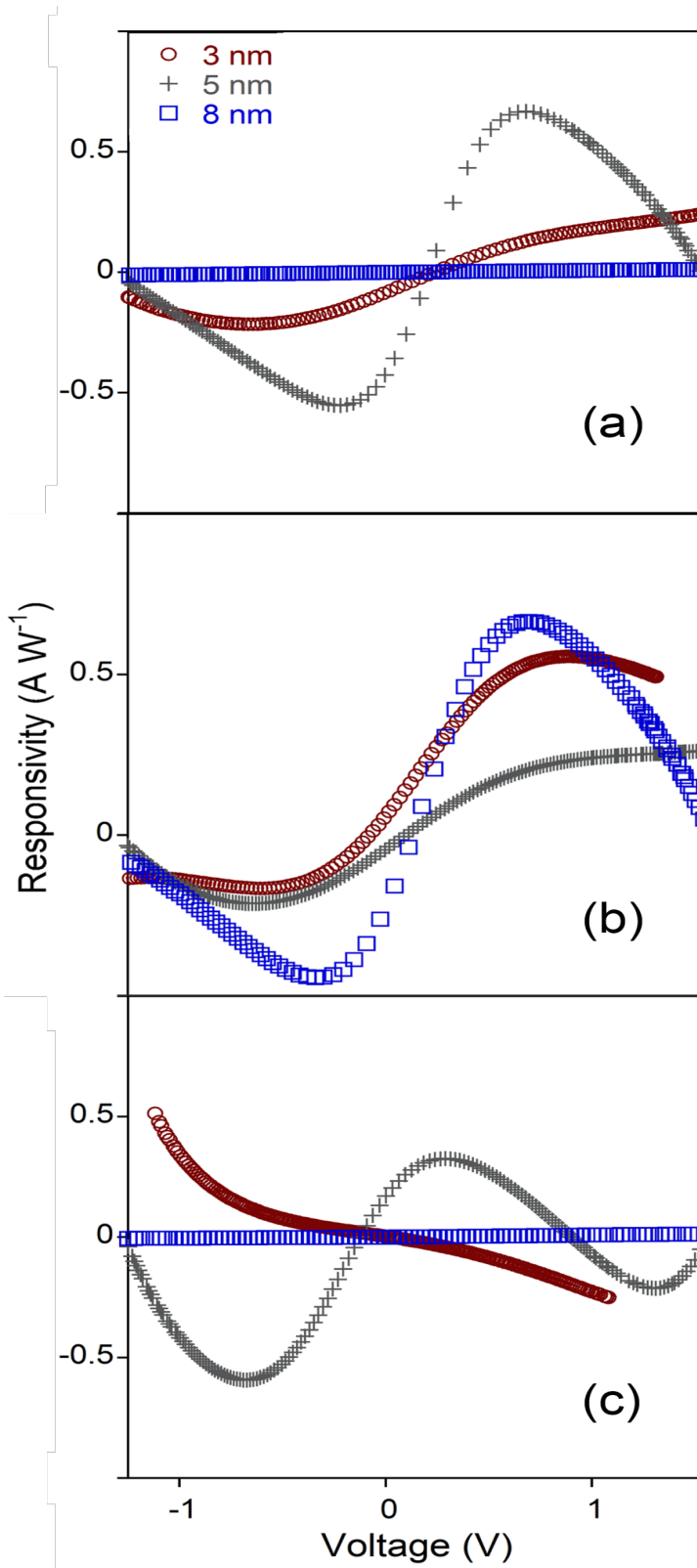


**Figure 7.2.** Responsivity plots for devices with (a) 50 nm Ca / 60 nm Al / 90 nm Ag, (b) 60 nm Al / 90 nm Ag, and (c) 200 nm Au top metal layers, respectively.

From the responsivity plots (Figure 7.2), it is evident that Ca and Al based diodes have shown some responsivity while Au based diodes have poor responsivity. While looking at the effect of diode thickness on responsivity, it can be inferred that 5 nm thick oxide diodes have shown promising responsivity in all the cases.

### 7.3 Asymmetry

Rectification requires an imbalance between the forward and reverse currents formed during the positive and negative cycles of the AC potential at the junction. There are different ways to implement electrical asymmetry such as material asymmetry, thermal or geometric asymmetry. We opted for material asymmetry which was insured by the using metals of different workfunction in our MIM diode i.e. MWCNT-Al<sub>2</sub>O<sub>3</sub>-Metal diode.

Diode asymmetry (A) is defined as follows

$$A = \left| \frac{I(V)}{I(-V)} \right| \quad (3)$$

A greater asymmetry in the I–V curve is important, thus MIM diodes need to be fabricated with strong non-linearity to obtain detectors with large response, especially for solar rectenna as it is desirable to operate the rectenna without applying an external DC bias [55]. But there is a tradeoff between these parameters. Different workfunction metals on both side of diode give rise to asymmetry [103] resulting in higher responsivity [104] while low diode resistance requires low barrier heights on both sides, which reduces asymmetry [23].

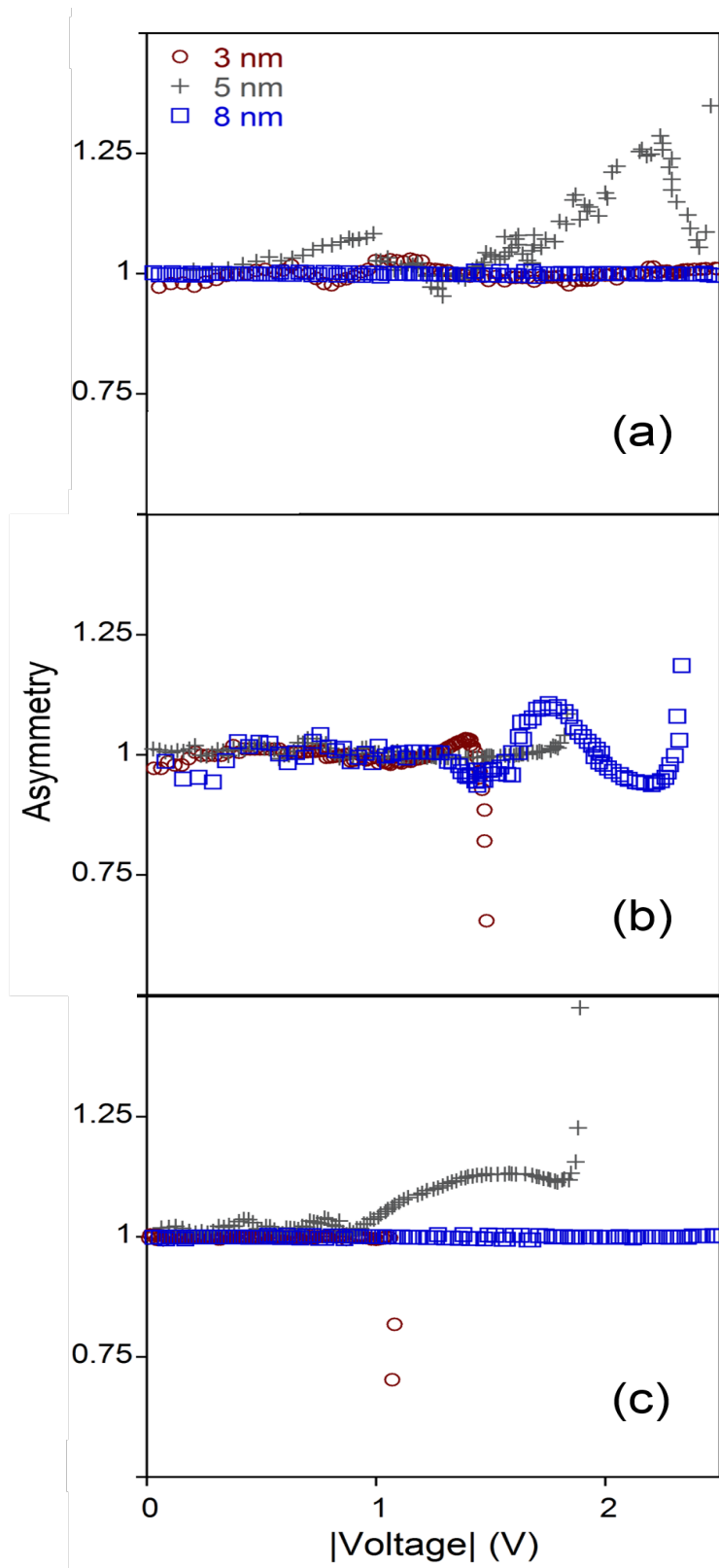


**Figure. 7.3.** Asymmetry plots for devices with (a) 50 nm Ca / 60 nm Al / 90 nm Ag, (b) 60 nm Al / 90 nm Ag, and (c) 200 nm Au top metal layers, respectively.

The MWNT-Al<sub>2</sub>O<sub>3</sub>-Ca diode has a workfunction difference of 2.1 eV, while for Al coated diode workfunction difference is only 0.7 eV. So Ca devices have high asymmetry resulting in low turn-on voltage (Figure 7.3), which is a very much favorable condition for rectification.

While looking at all of these parameters we have to decide the best thickness of insulator, which gives us a balance of all the above mentioned parameters of diode for defining high performance diode. Table 7.1 gives an overview of all these parameters.

**Table. 7.1.** Comparison of diode parameters (Conduction is given as an inverse of zero-bias resistance for an ease of description).

Thickness	Metal	Conductance	Responsivity	Asymmetry
3nm	Ca	↓	↔	↔
	Al	↔	↔	↓
	Au	↑	↓	↓
5nm	Ca	↓	↑	↑
	Al	↑	↓	↑
	Au	↔	↑	↑
8nm	Ca	↓	↔	↓
	Al	↑	↑	↔
	Au	↓	↔	↔

↑ High  
↔ Average  
↓ Low

Thus 5nm thickness of insulator gives the ideal situation with higher responsivity, asymmetry and average conduction of the diode. 5nm is enough thickness to ensure efficient tunneling while being thick enough to ensure there is no penetration of top metal through the insulator layer to short the device.

## 7.4 Coupling Efficiency

As discussed earlier, antenna-diode coupling is the significant factor for efficient rectennas at optical frequencies. The overall efficiency of the rectenna is proportional to the square of coupling efficiency ( $\eta_{\text{coupling}}$ ) [23], [105], which is the ratio of ac power delivered to the diode resistance ( $P_{AC,R_D}$ ) to the power sourced by antenna ( $P_{V_A}$ ) [8].

$$\eta_{\text{coupling}} = \frac{P_{AC,R_D}}{P_{V_A}} = \frac{4(R_A R_D / (R_A + R_D)^2)}{1 + (\omega (R_A R_D / (R_A + R_D)) C_D)^2} \quad (4)$$

From this relation it can be inferred that for the highest coupling efficiency diode resistance ( $R_D$ ) should be equal to the resistance of antenna ( $R_A$ ). The ideal condition to deal with these constraints simultaneously would be  $\omega(R_A || R_D)C_D \ll 1$  and  $R_A = R_D$ . Which results as following

$$R_D C_D \ll \frac{2}{\omega} \quad (5)$$

For antenna-diode impedance match, we brought diode resistance significantly below to  $300 \Omega\text{cm}^2$  for 5nm insulator thickness and even lower to  $100 \Omega\text{cm}^2$  for 3nm while previously reported results for this kind of device showed  $7.5 \text{ k}\Omega\text{cm}^2$  [7]. But, if we apply above-mentioned ideal conditions for highest coupling efficiency to our device, as  $R_D \gg R_A$  then  $R_A C_D$  becomes an important factor to consider [54]. In our design  $R_A = 100\Omega$  with the corresponding  $C_D = 2.7 \text{ aF}$  at 5nm thickness of insulator, then  $R_A C_D = 2.7 \times 10^{-16}$  which is smaller than  $\frac{2}{\omega} \cong 5.4 \times 10^{-16}$ , which shows that our device can reach to ideal coupling efficiency. If we look at the difference between diode resistance and

antenna resistance, there is still a lot of work required to reach at the ideal efficiency. Our experiments proved to decrease resistance substantially but there is still need for improvement.

## CHAPTER 8

### CONCLUSIONS

This work primarily reduces rectenna-diode impedance mismatch. In our design MWCNT antenna is already an integral part of the diode, which ensures efficient connection between antenna and diode. So we just focused on MWCNT-Al<sub>2</sub>O<sub>3</sub>-metal diode contact resistances. Contact resistances are the major contributors for overall diode resistance. We started with top metal and analyzed different metals of varying thicknesses to find the best combination with lowest resistance. After selecting best top metal thickness i.e. 200 nm, we considered the MWCNT-Oxide interface. MWCNT has a hemi-spherical tip, which limits the bonding to only the outer wall of MWCNT and blocks access to inner walls. To have better bonding at the interface we opened the MWCNT tips, which made all the inner walls available for bonding and led to better wettability resulting in reduced contact resistance. Plasma treatment to open CNT tips also enhanced total emission current density and decreased the turn-on field. Then we introduced Al<sub>2</sub>O<sub>3</sub> (insulator) in the structure to fabricate a complete rectenna device. Along with the oxide addition, new combinations of top metals were introduced to ensure the rectification. The oxide thickness was carefully optimized for tunneling of electrons at THz frequencies to ensure rectification in the optical range. Among the top metals, it was found that MWCNT-Al<sub>2</sub>O<sub>3</sub>-Ca diode with 5nm oxide thickness is the best combination.

In comparison to the previous studies of resistance for optical rectenna, this study led to a substantial reduction in diode resistance up to 300  $\Omega\text{cm}^2$  for 5nm thick oxide and 100

$\Omega\text{cm}^2$  for 3nm thickness of oxide in MWCNT- $\text{Al}_2\text{O}_3$ -Ca diode. The reduction in the diode resistance ensured efficient coupling of antenna and diode, which resulted in the operation of our optical rectenna in the visible range at 585 THz frequencies.

## **CHAPTER 9**

### **RECOMMENDATIONS**

Our study is based on reducing the interface resistance of our MWCNT-Oxide-Metal diode to have better coupling with the antenna. We have been successful in identifying the different contributors towards overall resistance of the diode and have been able to substantially reduce this resistance. However, there is room for a lot of improvements to make this optical rectenna technology a via-able option on the commercial level. Following recommendations may help realizing this concept:

- For our specified MWCNT diode, there are still possibilities to reach lower resistance. One possibility is to use graphitic carbon deposited at CNT interface [22, 91]. A layer of annealed graphitic carbon at the open tip CNTs may improve wettability substantially and has negligibly small intrinsic resistance [106]. Thus by decreasing interface resistances, coupling efficiency could be substantially increased which will lead to higher conversion efficiency and potential applications of optical rectenna devices.
- MWCNTs have lower electron density in comparison to the top metal, which may cause the leakage of current in the opposite direction. This can be handled with either doping of MWCNTs or the ALD of thin films of high electron density metals e.g. Au or Ag.
- Investigate the leakage current for 3nm insulator thickness as if we can use the 3nm thickness of insulator, it will overall performance of diode with low zero-

bias resistance and higher responsivity.

- As this whole study is dependent on measuring the contact/sheet resistance of different interfaces, it is really important to have a standard process of resistance measure, which can give the precise measures. 4-probe system helped but adjusting the probes over a thin metal layer while ensuring it doesn't poke through the layer to short the device is a difficult and ambiguous process. We can use laser ablation technique of measuring contact resistance between an individual nanotube and a deposited film [107].
- In our devices, oxidation of the top metal is a big issue. This oxidation impacts the resistance measurements, so the characterization process of the devices should be carried out in the inert environment to get the precise measurements.
- While depositing top-metals, to complete the 200nm top metal thickness, Ag was used as the filler metal for Al because of the 60nm maximum evaporation limit forced by the evaporator. E.g. in Ca/Al based diode, actual design was to deposit 50nm Ca and coat it with 150nm Al but because of 60nm deposition limit of Al the total thickness was achieved by 90nm Ag and same happened for 200 nm Al, where after 60nm deposition the rest was filled with Ag. This may have impact on the morphology of top metal resulting in poor rectification.
- Vital variations from the commanded thicknesses have been observed in Denton E-Beam Evaporator depositions. So it is suggested to measure the thicknesses of deposited oxide or metal layer to ensure the precise fabrication as it affects overall device performance.

## APPENDIX A

### RESISTANCE TABLES

#### A.1. Influence of Top Metal Thickness on Contact Resistance

**Table A.1.** Average contact resistances for various top metals and thicknesses

Thickness (nm)	Average Resistance ( $\Omega \text{ cm}^2$ )			
	Ti	Al	Ni	Au
50	3.4534	203.3790	19.2212	13.1966
200	0.3993	1.4680	3.0860	8.5306
500	0.7553	1.6353	1.3167	6.0690

#### A.2. Influence of Top Metal Thickness on Contact Resistance

**Table A.2.** Percentage change in average contact resistance after opening CNT tips for all four top metals (Ti, Al, Ni, Au) each of 200 nm thickness.

Metal	Closed Tip Resistance ( $\Omega \text{ cm}^2$ )	Open Tip Resistance ( $\Omega \text{ cm}^2$ )	% Change in Resistance
Ti	0.3993	0.1876	- 51.89
Al	1.4680	34.3427	2239.42
Ni	3.0860	2.8904	- 6.33
Au	8.5306	8.2292	- 3.53

### A.3. Influence of Insulator Thickness on Zero-bias Resistance

**Table A.3.** Effect of oxide thicknesses on zero-bias resistance of diodes of Ca/Al, Al, and Au based diodes

Oxide Thickness (nm)	Zero Bias Resistance ( $k\Omega \text{ cm}^2$ )		
	Ca/Al	Al	Au
3	0.1004	0.0704	0.0261
5	0.3736	0.2010	0.2895
8	2.3367	0.5518	2.3451

## APPENDIX B

### POLYNOMIAL EQUATIONS

#### B.1. Example Equations Fitted to I-V Curves

The following equations are corresponding to resistance and responsivity plot in Figures 6.7 (b) and 7.2 (b) respectively for 60nm Al/90nm Ag (5nm Oxide) device. Where equation A1 is fitted to I-V plot in Figure 6.6 (b) of this device as current being independent factor and equation A3 is fitted as voltage being independent factor. While equation A2 is first derivative of A1 and A4, A5 are 1<sup>st</sup> and 2<sup>nd</sup> derivatives respectively of equation A3.

Voltage (V) = multiple of Current (I)

$$V = 6.855321063*10^{-8} I^6 + 2.202965013*10^{-6} I^5 - 1.654093427*10^{-5} I^4 - \quad (A1) \\ 6.136709135*10^{-4} I^3 + 1.060359915*10^{-3} I^2 + 2.010207082*10^{-1} I - 1.661528359*10^{-3}$$

$$R = \frac{dV}{dI} = (15539202440266323* I^5)/37778931862957161709568 + \quad (A2) \\ (13004010175407115* I^4)/1180591620717411303424 - (4882022099499867* \\ I^3)/73786976294838206464 - (8490172715110539* I^2)/4611686018427387904 + \\ (2445023497253177* I)/1152921504606846976 + \\ 3621267146173093/18014398509481984$$

Current (I) = multiple of voltage (V)

$$I = 1.381612032*10^{-2} V^6 - 5.016514651*10^{-2} V^5 - 1.380257513*10^{-3} V^4 + \quad (A3) \\ 6.335493523*10^{-1} V^3 - 1.190373904*10^{-1} V^2 + 4.851751807 V + 5.116177598*10^{-3}$$

$$\begin{aligned} \frac{dI}{dV} = & (2986669167593181 * V^5) / 36028797018963968 - & (A4) \\ & (18073898810353785 * V^4) / 72057594037927936 - \\ & (6365314274531459 * V^3) / 1152921504606846976 + \\ & (17119515761634597 * V^2) / 9007199254740992 - \\ & (8577547952777541 * V) / 36028797018963968 + \\ & 5462586907524833 / 1125899906842624 \end{aligned}$$

$$\begin{aligned} \frac{d^2I}{d^2V} = & (14933345837965905 * V^4) / 36028797018963968 - & (A5) \\ & (18073898810353785 * V^3) / 18014398509481984 - \\ & (19095942823594377 * V^2) / 1152921504606846976 + \\ & (17119515761634597 * V) / 4503599627370496 - \\ & 8577547952777541 / 36028797018963968 \end{aligned}$$

## REFERENCES

- [1] S. Grover and G. Moddel, "Engineering the current–voltage characteristics of metal–insulator–metal diodes using double-insulator tunnel barriers," *Solid-State Electronics*, vol. 67, pp. 94-99, 2012.
- [2] D. M. Chapin, C. S. Fuller, and G. L. Pearson, "Solar energy converting apparatus," ed: Google Patents, 1957.
- [3] W. Shockley and H. J. Queisser, "Detailed Balance Limit of Efficiency of p - n Junction Solar Cells," *Journal of Applied Physics*, vol. 32, pp. 510-519, 1961.
- [4] C. H. Henry, "Limiting efficiencies of ideal single and multiple energy gap terrestrial solar cells," *Journal of Applied Physics*, vol. 51, pp. 4494-4500, 1980.
- [5] R. L. Bailey, "A proposed new concept for a solar-energy converter," *Journal of Engineering for Power*, vol. 94, pp. 73-77, 1972.
- [6] W. C. Brown, "Experiments involving a microwave beam to power and position a helicopter," *Aerospace and Electronic Systems, IEEE Transactions on*, pp. 692-702, 1969.
- [7] A. Sharma, V. Singh, T. L. Bougher, and B. A. Cola, "A carbon nanotube optical rectenna," *Nature nanotechnology*, 2015.
- [8] S. Grover and G. Moddel, "Metal single-insulator and multi-insulator diodes for rectenna solar cells," in *Rectenna Solar Cells*, ed: Springer, 2013, pp. 89-109.
- [9] S. Wang, T. Gustafson, and T. Izawa, "Coupling characteristics of thin-film metal-oxide-metal diodes at 10.6 microns," *Applied Physics Letters*, vol. 27, pp. 481-483, 1975.
- [10] B. Tiwari, J. A. Bean, G. Szakmany, G. H. Bernstein, P. Fay, and W. Porod, "Controlled etching and regrowth of tunnel oxide for antenna-coupled metal-oxide-metal diodes," *Journal of vacuum science & technology. B, Microelectronics and nanometer structures*, vol. 27, p. 2153, 2009.

- [11] S. Marchetti, P. Sandri, and R. Simili, "Theoretical and experimental responsivity of FIR antenna coupled metal-insulator-metal detectors," *International journal of infrared and millimeter waves*, vol. 18, pp. 2161-2175, 1997.
- [12] P. C. Hobbs, R. B. Laibowitz, F. R. Libsch, N. C. LaBianca, and P. P. Chiniwalla, "Efficient waveguide-integrated tunnel junction detectors at 1.6  $\mu\text{m}$ ," *Optics express*, vol. 15, pp. 16376-16389, 2007.
- [13] A. M. Marks, "Device for conversion of light power to electric power," ed: Google Patents, 1984.
- [14] G. H. Lin, R. Abdu, and J. O. M. Bockris, "Investigation of resonance light absorption and rectification by subnanostructures," *Journal of applied physics*, vol. 80, pp. 565-568, 1996.
- [15] D. K. Kotter, S. D. Novack, W. Slafer, and P. Pinhero, "Theory and manufacturing processes of solar nanoantenna electromagnetic collectors," *Journal of Solar Energy Engineering*, vol. 132, p. 011014, 2010.
- [16] M. Midrio, M. Romagnoli, S. Boscolo, C. De Angelis, A. Locatelli, D. Modotto, *et al.*, "Flared Monopole Antennas for 10-Radiation," *Quantum Electronics, IEEE Journal of*, vol. 47, pp. 84-91, 2011.
- [17] G. Moddel and S. Grover, *Rectenna Solar Cells*: Springer, 2013.
- [18] S. Joshi and G. Moddel, "Efficiency limits of rectenna solar cells: Theory of broadband photon-assisted tunneling," *Applied Physics Letters*, vol. 102, p. 083901, 2013.
- [19] E. Donchev, J. S. Pang, P. M. Gammon, A. Centeno, F. Xie, P. K. Petrov, *et al.*, "The rectenna device: From theory to practice (a review)," *MRS Energy & Sustainability*, vol. 1, p. E1, 2014.
- [20] Y. Wang, K. Kempa, B. Kimball, J. Carlson, G. Benham, W. Li, *et al.*, "Receiving and transmitting light-like radio waves: Antenna effect in arrays of aligned carbon nanotubes," *Applied physics letters*, vol. 85, pp. 2607-2609, 2004.

- [21] K. Kempa, J. Rybczynski, Z. Huang, K. Gregorczyk, A. Vidan, B. Kimball, *et al.*, "Carbon nanotubes as optical antennae," *Advanced Materials*, vol. 19, pp. 421-426, 2007.
- [22] S. Kim, D. D. Kulkarni, K. Rykaczewski, M. Henry, V. V. Tsukruk, and A. G. Fedorov, "Fabrication of an ultralow-resistance ohmic contact to MWCNT-metal interconnect using graphitic carbon by electron beam-induced deposition (EBID)," *Nanotechnology, IEEE Transactions on*, vol. 11, pp. 1223-1230, 2012.
- [23] B. J. Eliasson, "Metal-insulator-metal diodes for solar energy conversion," University of Colorado, 2001.
- [24] K. D. Sattler, *Handbook of nanophysics: functional nanomaterials*: CRC Press, 2010.
- [25] R. Corkish, M. Green, and T. Puzzer, "Solar energy collection by antennas," *Solar Energy*, vol. 73, pp. 395-401, 2002.
- [26] Y.-J. Ren, M. F. Farooqui, and K. Chang, "A compact dual-frequency rectifying antenna with high-orders harmonic-rejection," *Antennas and Propagation, IEEE Transactions on*, vol. 55, pp. 2110-2113, 2007.
- [27] J. O. McSpadden, L. Fan, and K. Chang, "Design and experiments of a high-conversion-efficiency 5.8-GHz rectenna," *Microwave Theory and Techniques, IEEE Transactions on*, vol. 46, pp. 2053-2060, 1998.
- [28] C.-H. K. Chin, Q. Xue, and C. H. Chan, "Design of a 5.8-GHz rectenna incorporating a new patch antenna," *Antennas and Wireless Propagation Letters, IEEE*, vol. 4, pp. 175-178, 2005.
- [29] V. Mlinar, "Engineered nanomaterials for solar energy conversion," *Nanotechnology*, vol. 24, p. 042001, 2013.
- [30] N. Tesla, "System of transmission of electrical energy," ed: Google Patents, 1900.
- [31] O. E.C., *Microwave Power Engineering* vol. I, II. New York: Academic Press, 1968.

- [32] P. E. Glaser, "Power from the Sun: Its Future," *Science*, vol. 162, pp. 857-861, 1968-11-22 00:00:00 1968.
- [33] O. EnergyResearch, "Satellite Power Systems (SPS) Concept Development and Evaluation Program Preliminary Assessment."
- [34] K. N. Shimokura N., Shinohara N., and Matsumoto H., "Point-to-point microwave power transmission experiment.," *international electrical engineering journal of japan*, vol. 116(6), pp. 648–653 1996.
- [35] N. Shinohara and H. Matsumoto, "Experimental study of large rectenna array for microwave energy transmission," *Microwave Theory and Techniques, IEEE Transactions on*, vol. 46, pp. 261-268, 1998.
- [36] J. O. McSpadden, F. E. Little, M. B. Duke, and A. Ignatiev, "An in-space wireless energy transmission experiment," in *Energy Conversion Engineering Conference, 1996. IECEC 96., Proceedings of the 31st Intersociety*, 1996, pp. 468-473.
- [37] T.-W. Yoo and K. Chang, "Theoretical and experimental development of 10 and 35 GHz rectennas," *Microwave Theory and Techniques, IEEE Transactions on*, vol. 40, pp. 1259-1266, 1992.
- [38] L. W. Epp, A. R. Khan, H. K. Smith, and R. P. Smith, "A compact dual-polarized 8.51-GHz rectenna for high-voltage (50 V) actuator applications," *Microwave Theory and Techniques, IEEE Transactions on*, vol. 48, pp. 111-120, 2000.
- [39] Y. Fujino, M. FUJITA, K. Nobuyuki, H. MATSUMOTO, K. KAWABATA, H. SAWADA, *et al.*, "A driving test of a small DC motor with a rectenna array," *IEICE Transactions on Communications*, vol. 77, pp. 526-528, 1994.
- [40] J. A. Hagerty, F. B. Helmbrecht, W. H. McCalpin, R. Zane, and Z. B. Popović, "Recycling ambient microwave energy with broad-band rectenna arrays," *Microwave Theory and Techniques, IEEE Transactions on*, vol. 52, pp. 1014-1024, 2004.
- [41] X.-X. Yang, C. Jiang, A. Z. Elsherbeni, F. Yang, and Y.-Q. Wang, "A novel compact printed rectenna for data communication systems," *Antennas and Propagation, IEEE Transactions on*, vol. 61, pp. 2532-2539, 2013.

- [42] D. Y. Goswami, S. Vijayaraghavan, S. Lu, and G. Tamm, "New and emerging developments in solar energy," *Solar energy*, vol. 76, pp. 33-43, 2004.
- [43] R. L. Bailey and P. S. Callahan, "Electromagnetic wave energy conversion research," 1975.
- [44] A. M. Marks, "Ordered dipolar light-electric power converter," ed: Google Patents, 1986.
- [45] A. M. Marks, "Femto diode and applications," ed: Google Patents, 1988.
- [46] A. M. Marks, "Lighting devices with quantum electric/light power converters," ed: Google Patents, 1990.
- [47] G. T. K. a. B. K., "Metal-oxide-metal optical diodes," *Ames. R.C. Rsch. Review, NASA J.* 1974.
- [48] U. o. Missouri, "New solar technology could break photovoltaic limits," ed. Columbia, MO: MU News Bureau, 2011.
- [49] M. Pasquali. Rectenna (rectifying antenna) behavior of carbon nanotubes and gold nanowires [Online].
- [50] C. Poitras, "UConn Professor's Patented Technique Key to New Solar Power Technology," ed. University of Connecticut UConn Communications, 2013.
- [51] M. Nagae, "Response time of metal-insulator-metal tunnel junctions," *Japanese Journal of Applied Physics*, vol. 11, p. 1611, 1972.
- [52] H. Riccius, "Improved metal-insulator-metal point-contact diodes for harmonic generation and mixing," *Applied physics*, vol. 17, pp. 49-52, 1978.
- [53] N. Alimardani, E. William Cowell, J. F. Wager, J. F. Conley, D. R. Evans, M. Chin, *et al.*, "Impact of electrode roughness on metal-insulator-metal tunnel diodes with atomic layer deposited Al<sub>2</sub>O<sub>3</sub> tunnel barriers," *Journal of Vacuum Science & Technology A*, vol. 30, p. 01A113, 2012.

- [54] A. Sanchez, C. Davis Jr, K. Liu, and A. Javan, "The MOM tunneling diode: theoretical estimate of its performance at microwave and infrared frequencies," *Journal of Applied Physics*, vol. 49, pp. 5270-5277, 1978.
- [55] S. Grover and G. Moddel, "Applicability of metal/insulator/metal (MIM) diodes to solar rectennas," *Photovoltaics, IEEE Journal of*, vol. 1, pp. 78-83, 2011.
- [56] B. J. Eliasson and G. Moddel, "Metal-oxide electron tunneling device for solar energy conversion," ed: Google Patents, 2003.
- [57] G. Moddel and B. J. Eliasson, "High speed electron tunneling device and applications," ed: Google Patents, 2004.
- [58] B. Hegyi, Á. Csurgay, and W. Porod, "Investigation of the nonlinearity properties of the DC IV characteristics of metal-insulator-metal (MIM) tunnel diodes with double-layer insulators," *Journal of Computational Electronics*, vol. 6, pp. 159-162, 2007.
- [59] P. Maraghechi, A. Foroughi-Abari, K. Cadien, and A. Elezzabi, "Enhanced rectifying response from metal-insulator-insulator-metal junctions," *Applied Physics Letters*, vol. 99, p. 253503, 2011.
- [60] N. M. Miskovsky, P. H. Cutler, A. Mayer, B. L. Weiss, B. Willis, T. E. Sullivan, *et al.*, "Nanoscale devices for rectification of high frequency radiation from the infrared through the visible: a new approach," *Journal of Nanotechnology*, vol. 2012, 2012.
- [61] P. C. Hobbs, R. B. Laibowitz, and F. R. Libsch, "Ni–NiO–Ni tunnel junctions for terahertz and infrared detection," *Applied optics*, vol. 44, pp. 6813-6822, 2005.
- [62] P. Biagioni, J.-S. Huang, and B. Hecht, "Nanoantennas for visible and infrared radiation," *Reports on Progress in Physics*, vol. 75, p. 024402, 2012.
- [63] M. J. Estes and G. Moddel, "Surface plasmon devices," ed: Google Patents, 2006.
- [64] G. Moddel, "Geometric diode, applications and method," ed: Google Patents, 2014.

- [65] Z. Zhu, S. Joshi, S. Grover, and G. Moddel, "Graphene geometric diodes for terahertz rectennas," *Journal of Physics D: Applied Physics*, vol. 46, p. 185101, 2013.
- [66] Z. Zhu, S. Grover, K. Krueger, and G. Moddel, "Optical rectenna solar cells using graphene geometric diodes," in *Photovoltaic Specialists Conference (PVSC), 2011 37th IEEE*, 2011, pp. 002120-002122.
- [67] S. Joshi, Z. Zhu, S. Grover, and G. Moddel, "Infrared optical response of geometric diode rectenna solar cells," in *Photovoltaic Specialists Conference (PVSC), 2012 38th IEEE*, 2012, pp. 002976-002978.
- [68] G. Moddel, Z. Zhu, S. Grover, and S. Joshi, "Ultrahigh speed graphene diode with reversible polarity," *Solid State Communications*, vol. 152, pp. 1842-1845, 2012.
- [69] S. Grover, "Diodes for optical rectennas," UNIVERSITY OF COLORADO AT BOULDER, 2011.
- [70] Z. Ren, K. Kempa, and Y. Wang, "Solar cells using arrays of optical rectennas," ed: Google Patents, 2005.
- [71] H. Ago, T. Kugler, F. Cacialli, W. R. Salaneck, M. S. Shaffer, A. H. Windle, *et al.*, "Work functions and surface functional groups of multiwall carbon nanotubes," *The Journal of Physical Chemistry B*, vol. 103, pp. 8116-8121, 1999.
- [72] S. Suzuki, C. Bower, Y. Watanabe, and O. Zhou, "Work functions and valence band states of pristine and Cs-intercalated single-walled carbon nanotube bundles," *Applied Physics Letters*, vol. 76, pp. 4007-4009, 2000.
- [73] M. W. Knight, H. Sobhani, P. Nordlander, and N. J. Halas, "Photodetection with active optical antennas," *Science*, vol. 332, pp. 702-704, 2011.
- [74] A. Giugni, B. Torre, A. Toma, M. Francardi, M. Malerba, A. Alabastri, *et al.*, "Hot-electron nanoscopy using adiabatic compression of surface plasmons," *Nature nanotechnology*, vol. 8, pp. 845-852, 2013.
- [75] C.-P. Juan, C.-C. Tsai, K.-H. Chen, L.-C. Chen, and H.-C. Cheng, "Effects of high-density oxygen plasma posttreatment on field emission properties of carbon

- nanotube field-emission displays," *Japanese journal of applied physics*, vol. 44, p. 8231, 2005.
- [76] J. Nguyen, T. Bougher, P. P. S. S. Abadi, A. Sharma, S. Graham, and B. Cola, "Postgrowth microwave treatment to align carbon nanotubes," *Journal of Micro and Nano-Manufacturing*, vol. 1, p. 014501, 2013.
- [77] J. G. Simmons, "Electric tunnel effect between dissimilar electrodes separated by a thin insulating film," *Journal of applied physics*, vol. 34, pp. 2581-2590, 1963.
- [78] H. Choi, J. Gong, Y. Lim, K. H. Im, and M. Jeon, "Effects of the electrical conductivity and orientation of silicon substrate on the synthesis of multi-walled carbon nanotubes by thermal chemical vapor deposition," *Nanoscale research letters*, vol. 8, pp. 1-6, 2013.
- [79] W. Su, T. Leung, and C. Chan, "Work function of single-walled and multiwalled carbon nanotubes: first-principles study," *Physical Review B*, vol. 76, p. 235413, 2007.
- [80] H. Dai, "Carbon nanotubes: synthesis, integration, and properties," *Accounts of chemical research*, vol. 35, pp. 1035-1044, 2002.
- [81] M. Kumar and Y. Ando, *Carbon nanotube synthesis and growth mechanism*: INTECH Open Access Publisher, 2011.
- [82] C. J. Vasquez, "Oxide-coated vertically aligned carbon nanotube forests as thermal interface materials," 2014.
- [83] A. Magrez, J. W. Seo, R. Smajda, M. Mionić, and L. Forró, "Catalytic CVD synthesis of carbon nanotubes: towards high yield and low temperature growth," *Materials*, vol. 3, pp. 4871-4891, 2010.
- [84] R. Baker, P. Harris, R. Thomas, and R. Waite, "Formation of filamentous carbon from iron, cobalt and chromium catalyzed decomposition of acetylene," *Journal of catalysis*, vol. 30, pp. 86-95, 1973.
- [85] S. M. George, "Atomic layer deposition: an overview," *Chemical reviews*, vol. 110, pp. 111-131, 2009.

- [86] J. Lee, B. Min, K. Cho, S. Kim, J. Park, Y. Lee, *et al.*, "Al<sub>2</sub>O<sub>3</sub> nanotubes and nanorods fabricated by coating and filling of carbon nanotubes with atomic-layer deposition," *Journal of crystal growth*, vol. 254, pp. 443-448, 2003.
- [87] C. Herrmann, F. Fabreguette, D. Finch, R. Geiss, and S. George, "Multilayer and functional coatings on carbon nanotubes using atomic layer deposition," *Applied Physics Letters*, vol. 87, p. 123110, 2005.
- [88] D. R. Prof. Erich Bergmann. (2013, 20 April ). Corrosion protection with perfect atomic layers. *Oberflächen POLYSURFACES*.
- [89] S. Swapp. (2016, Scanning Electron Microscopy. *Integrating Research and Education*.
- [90] F. Smits, "Measurement of sheet resistivities with the four - point probe," *Bell System Technical Journal*, vol. 37, pp. 711-718, 1958.
- [91] Y. Chai, A. Hazeghi, K. Takei, H.-Y. Chen, P. C. Chan, A. Javey, *et al.*, "Low-resistance electrical contact to carbon nanotubes with graphitic interfacial layer," *Electron Devices, IEEE Transactions on*, vol. 59, pp. 12-19, 2012.
- [92] Y. Zhang, N. W. Franklin, R. J. Chen, and H. Dai, "Metal coating on suspended carbon nanotubes and its implication to metal-tube interaction," *Chemical Physics Letters*, vol. 331, pp. 35-41, 2000.
- [93] J. Chang, H. Kuo, I. Leu, and M. Hon, "The effects of thickness and operation temperature on ZnO: Al thin film CO gas sensor," *Sensors and actuators B: Chemical*, vol. 84, pp. 258-264, 2002.
- [94] A. Mayadas and M. Shatzkes, "Electrical-resistivity model for polycrystalline films: the case of arbitrary reflection at external surfaces," *Physical review B*, vol. 1, p. 1382, 1970.
- [95] M. J. Madou, *Fundamentals of microfabrication: the science of miniaturization*: CRC press, 2002.
- [96] W. A. De Heer, A. Chatelain, and D. Ugarte, "A carbon nanotube field-emission electron source," *Science*, vol. 270, pp. 1179-1180, 1995.

- [97] S. Krishnan, "Design, fabrication and characterization of thin-film MIM diodes for rectenna array," University of South Florida, 2004.
- [98] M. D. Fayer, *Elements of quantum mechanics*: Oxford University Press New York, 2001.
- [99] C. Fumeaux, W. Herrmann, F. Kneubühl, and H. Rothuizen, "Nanometer thin-film Ni–NiO–Ni diodes for detection and mixing of 30 THz radiation," *Infrared physics & technology*, vol. 39, pp. 123-183, 1998.
- [100] I. Wilke, Y. Oppliger, W. Herrmann, and F. Kneubühl, "Nanometer thin-film Ni–NiO–Ni diodes for 30 THz radiation," *Applied Physics A*, vol. 58, pp. 329-341, 1994.
- [101] S. Krishnan, H. La Rosa, E. Stefanakos, S. Bhansali, and K. Buckle, "Design and development of batch fabricatable metal–insulator–metal diode and microstrip slot antenna as rectenna elements," *Sensors and Actuators A: Physical*, vol. 142, pp. 40-47, 2008.
- [102] J. Tucker and M. Millea, "Photon detection in nonlinear tunneling devices," *Applied Physics Letters*, vol. 33, pp. 611-613, 1978.
- [103] J. A. Bean, B. Tiwari, G. H. Bernstein, P. Fay, and W. Porod, "Thermal infrared detection using dipole antenna-coupled metal-oxide-metal diodes," *Journal of Vacuum Science & Technology B*, vol. 27, pp. 11-14, 2009.
- [104] J. A. Bean, A. Weeks, and G. D. Boreman, "Performance optimization of antenna-coupled tunnel diode infrared detectors," *Quantum Electronics, IEEE Journal of*, vol. 47, pp. 126-135, 2011.
- [105] S. Grover, O. Dmitriyeva, M. J. Estes, and G. Moddel, "Traveling-wave metal/insulator/metal diodes for improved infrared bandwidth and efficiency of antenna-coupled rectifiers," *Nanotechnology, IEEE Transactions on*, vol. 9, pp. 716-722, 2010.
- [106] L. Ci, Z. Ryu, N. Y. Jin-Phillipp, and M. Rühle, "Investigation of the interfacial reaction between multi-walled carbon nanotubes and aluminum," *Acta Materialia*, vol. 54, pp. 5367-5375, 2006.

- [107] C. Lan, P. Srisungsitthisunti, P. B. Amama, T. S. Fisher, X. Xu, and R. G. Reifenberger, "Measurement of metal/carbon nanotube contact resistance by adjusting contact length using laser ablation," *Nanotechnology*, vol. 19, p. 125703, 2008.